A priori and a posteriori analysis in large eddy simulation of the two-dimensional decaying turbulence using an explicit filtering approach

P. A. Perezhogin[1] † and A.V. Glazunov[1]

[1]Marchuk Institute of Numerical Mathematics of the Russian Academy of Sciences, Gubkin str., 8, Moscow, Russia

(Received xx; revised xx; accepted xx)

In this work, we consider turbulence closures of LES (large eddy simulation) type for classical decaying 2D turbulence in a priori and a posteriori experiments using an explicit filtering approach. LES closures for enstrophy dissipation and kinetic energy backscatter are proposed. According to Germano 1986 decomposition, subfilter-scale stress for Gaussian filter is decomposed into three parts: Leonard, cross and Reynolds stresses. Leonard stress can be computed directly. We show that an enstrophy transfer spectrum associated with cross stress can be approximated with bilaplacian viscosity, and Reynolds stress predominantly injects energy into large scales; thus, its approximation by a deconvolution procedure can be considered a kinetic energy backscatter model. We propose LES closure consisting of the three parts mentioned above and estimate its free parameters as follows. Eddy viscosity is found using a dynamic procedure, and backscatter power is determined from the new relation between energy and enstrophy exchange with subfilter scales. The proposed model has the following distinctive features: it reproduces energy and enstrophy spectral transfer and reproduces energy growth in accordance with the filtered DNS (direct numerical simulation) data. The optimal value of the filter to grid width ratio is found by analysing grid convergence of turbulence statistics. We show that the dynamic procedure in a priori and a posteriori experiments predicts significantly different eddy viscosities and suggest that the enstrophy dissipation model needs further improvement.

1. Introduction

The main purpose of this paper is to construct LES (large eddy simulation) parameterization of unresolved two-dimensional turbulence, which is formulated in physical space, can be used with low-order numerical schemes and provides the coarse-grid dynamics statistically close to filtered DNS (direct numerical simulation) data. Such parameterizations may be beneficial for mesoscale ocean LES (MOLES) models; see Fox-Kemper & Menemenlis (2008) for the comprehensive review of various approaches to include LES techniques in the ocean models based on the primitive equations. Evaluation of different viscosity kernels in MOLES are given by various authors (Griffies & Hallberg 2000; Pearson *et al.* 2017; Bachman *et al.* 2017; Graham & Ringler 2013). Although the extension of our findings to the primitive

† Email address for correspondence: pperezhogin@gmail.com

equations is not straightforward, they highlight the main challenges on the way to build LES closure for the two-dimensional turbulence. To clarify our motivation, we first give some basic definitions.

Time evolution of two-dimensional incompressible viscous fluid in dimensionless variables is governed by the equation:

$$\frac{\partial \omega}{\partial t} + \frac{\partial}{\partial x_j}\left(u_j \omega\right) = \frac{1}{Re}\nabla^2 \omega, \tag{1.1}$$

where Re – Reynolds number; ω, u_j – vorticity and velocity, respectively, $\nabla = \left(\frac{\partial}{\partial x_1}, \frac{\partial}{\partial x_2}\right)$, x_1 and x_2 – coordinates along orthogonal horizontal directions. Here and subsequently, summation over the repeated indices ($j = 1, 2$) is assumed. Velocity, vorticity and streamfunction ψ are expressed through each other as follows:

$$\nabla^2 \psi = \omega, \tag{1.2}$$

$$\omega = \frac{\partial u_2}{\partial x_1} - \frac{\partial u_1}{\partial x_2}, \tag{1.3}$$

$$(u_1, u_2) = \left(-\frac{\partial \psi}{\partial x_2}, \frac{\partial \psi}{\partial x_1}\right). \tag{1.4}$$

In the LES approach (Sagaut 2006), a spatial filter is applied to the governing equation (1.1):

$$\frac{\partial \overline{\omega}}{\partial t} + \frac{\partial}{\partial x_j}\left(\overline{u}_j \overline{\omega}\right) = \frac{1}{Re}\nabla^2 \overline{\omega} - \frac{\partial}{\partial x_j}\left(\sigma_j\right), \tag{1.5}$$

where the base filter of width $\overline{\Delta}$ is defined as a convolution with a filter kernel G:

$$\overline{\phi} = \int G(\boldsymbol{x} - \boldsymbol{x}', \overline{\Delta})\phi(\boldsymbol{x}')\mathrm{d}\boldsymbol{x}'. \tag{1.6}$$

LES equation (1.5) is unclosed, and subfilter-scale (SFS) stress

$$\sigma_j = \overline{u_j \omega} - \overline{u}_j \overline{\omega} \tag{1.7}$$

must be parameterized, i.e., expressed as a function of filtered fields, $\overline{\omega}$ and $\overline{u}_j$. Additionally, the classical formulation of SFS stress in velocity variables will be needed:

$$\tau_{ij} = \overline{u_i u_j} - \overline{u}_i \overline{u}_j. \tag{1.8}$$

Two of the most popular filters are Gaussian and sharp spectral. The Gaussian filter attenuates the shortwave band of the solution spectrum but does not change the number of degrees of freedom (i.e., the Fourier transform of the filter kernel satisfies $\widetilde{G}(\boldsymbol{k}) \neq 0$). Formally, it can be inverted on a DNS mesh (Langford & Moser 1999), and the exact SFS stress (1.7) can be found. In this case, the LES equation will correspond to the change of the model variables. Numerical discretization of the LES equation on a coarse mesh introduces an additional subgrid-scale (SGS) stress, which includes the contribution of the unresolved scales and scheme errors. SFS stress (1.7) computed for the sharp spectral filter is appropriate for the spectral schemes, and it is usually referred to as SGS stress. See articles (Carati *et al.* 2001; Winckelmans *et al.* 2001; Gullbrand & Chow 2003) for an exact definition of SFS and SGS stresses.

Subgrid-scale LES closures for the two-dimensional turbulence appropriate for the spectral schemes have been developed in papers (Frederiksen & Davies 1997; Frederiksen *et al.* 2003; Frederiksen & Kepert 2006; Zidikheri & Frederiksen 2009; Frederiksen *et al.* 2012; Kitsios

et al. 2013), and a detailed review is given in Frederiksen *et al.* (2017). Nonlinear interaction with the unresolved scales was found from the direct interaction approximation (DIA), eddy damped quasi-normal Markovian (EDQNM) turbulence models and DNS data. Based on these data, LES closures have been formulated in Fourier space, and they approximate the SGS energy transfer spectrum either by the eddy viscosity model with the coefficient depending on the wavenumber, or in combination with the stochastic backscatter model. In accordance with Kraichnan (1976) results, spectral eddy viscosity has a cusp behaviour with a maximum at the truncation wavenumber, while in large scales it is negative. The major finding of these works is that when LES closure simulates the SGS energy transfer spectrum and the numerical scheme is consistent with the definition of SGS stress (i.e., spectral scheme), the LES model in a posteriori experiments reproduces the kinetic energy spectrum of DNS up to the cutoff wavenumber. This result still holds for the multilevel quasi-geostrophic (QG) and primitive equations, and also for non-homogeneous and non-isotropic flows (see Frederiksen *et al.* 2017).

It was first recognized in Ghosal (1996) and later verified in Chow & Moin (2003) that if the base filter width equals the grid step (Δ_g) of the LES model, i.e., filter to grid width ratio is FGR $= \overline{\Delta}/\Delta_g = 1$, SFS closures should not be appropriate for low-order numerical schemes, because the power spectrum of numerical errors dominates the power spectrum of SFS stress as for the sharp spectral filter (Ghosal 1996), as for the Gaussian one (Chow & Moin 2003). The possible option to construct consistent closure is to retain the sharp spectral filter but include numerical errors in the definition of the SGS stress (Thuburn *et al.* 2014; Perezhogin *et al.* 2019). Numerical errors of second-order schemes significantly change the SGS stress energy transfer spectrum in the two-dimensional turbulence. A cusp behaviour near the truncation wavenumber disappears, in accordance with the T. Lund proposition that numerical schemes carry out implicit filtering of the governing equations (Lund 1997, 2003), justifying the use of low-order eddy viscosity models (Laplacian or bilaplacian) in practical computations with low-order numerical schemes, compared to the spectral computations. Another interesting finding, which is more important in view of a recent activity to construct kinetic energy backscatter (KEB) parameterizations for the two-dimensional turbulence (Jansen & Held 2014; Jansen *et al.* 2015; Grooms *et al.* 2015; Berloff 2018; Jansen *et al.* 2019; Juricke *et al.* 2019, 2020*b*,*a*; Perezhogin 2020), was that the shape of the SGS stress energy generation spectrum on a large scale (region of negative spectral eddy viscosity) depends significantly on the numerical discretization (Thuburn *et al.* 2014).

Recent advances in machine learning give rise to the subgrid models based on the artificial neural networks (ANNs), see Guan *et al.* (2021); Beck *et al.* (2019); Xie *et al.* (2020); Maulik *et al.* (2019). In various papers (Kurz & Beck 2020; Stoffer *et al.* 2020), it is emphasized that discretization errors must be included in the definition of the SGS stress, and it is shown that SGS stress can be predicted with high accuracy. A great success in this direction is that local dissipative operator can be tuned exactly for the numerical scheme used by projecting ANN SGS closure on the dissipative direction (Beck *et al.* 2019). However, it seems that accurate modelling of SGS dissipation consistent with low-order numerical schemes is debatable because without compensation of dispersion errors, these errors will distort small resolved scales. Compensation of dispersion errors by ANN SGS closures is also possible. However, it is not clear whether such an application of the ANN approach is more efficient in comparison with the improvement of numerical schemes.

To sum up the review given above, the discretization errors of low-order numerical schemes usually account for the major part of the SGS stress, and LES closure consistent with the numerical scheme should compensate these errors. In particular, the energy transfer spectrum associated with SGS stress depends strongly on the numerical scheme in a small-scale region

(enstrophy dissipation) and large-scale region (kinetic energy backscatter). This fact makes it difficult to construct an LES closure, which can be universally applied for different numerical schemes, grid resolutions and flow regimes. The role of numerical errors in LES closure can be attenuated using an explicit filtering approach (see Gullbrand & Chow 2003; Carati *et al.* 2001; Winckelmans *et al.* 2001; Lund 2003; Bose *et al.* 2010). In contrast to the implicit filtering approach, where computational grid and numerical scheme implicitly define the base filter (i.e., FGR $\approx$ 1), in the explicit filtering approach, the width of the base filter and/or its shape are explicitly defined, and the filter width is chosen to be larger than the mesh step (FGR $>$ 1). The major feature of properly constructed LES closure with explicit filtering is that it should give grid-independent turbulence statistics (Bose *et al.* 2010). The base filter can be included into the LES equation (1.5) in several ways. The filter can be applied to the momentum transport tensor (Moin & Kim 1982; Lund 2003; Bose *et al.* 2010) or to the solution at each time step (Lund 2003; Maulik & San 2017*c*). Additionally, the base filter can be used in partial reconstruction of SFS stress using the following popular procedures: an approximate deconvolution model (ADM, Gullbrand & Chow 2003; Stolz *et al.* 2001), a scale-similarity model (SSM, Bardina *et al.* 1980; Bardino *et al.* 1983; Meneveau & Katz 2000) or a nonlinear gradient model (NGM, Clark *et al.* 1979; Winckelmans *et al.* 2001). In the NGM model, we assume that the base filter has a finite second moment, and it is defined by the width, but its shape is unknown. Additionally, the base filter width can be explicitly put into the dynamic procedure (see Germano 1992).

In this paper, we assume that the base filter is Gaussian, its width is explicitly defined and larger than the grid step. We will refer to any LES closure as a closure with explicit filtering if it approximates the SFS stress with some accuracy and demonstrates grid-convergence of turbulence statistics. The quality of the LES closure is assessed by comparing grid-convergent turbulence statistics to the filtered DNS data. By reducing the grid resolution (with the fixed base filter width) in a posteriori experiments, we can determine when LES closure designed for Gaussian filter is unable to work properly due to presence of the discretization errors. Note that applying an explicit filtering approach does not generally imply the reduction of effective resolution of the LES model. Indeed, the smallest resolved scales are usually distorted by dispersion errors and must be filtered out.

The most popular LES closure in three-dimensional turbulence is the Laplacian eddy viscosity with the Smagorinsky coefficient (Smagorinsky 1963):

$$\nu = (C_S\overline{\Delta})^2|\overline{S}|, \tag{1.9}$$

where C_S and $|\overline{S}| = \sqrt{2\overline{S}_{ij}\overline{S}_{ij}}$ are Smagorinsky constant and modulus of resolved strain-rate tensor, $\overline{S}_{ij} = \frac{1}{2}\left(\frac{\partial\overline{u}_i}{\partial x_j} + \frac{\partial\overline{u}_j}{\partial x_i}\right)$. The Smagorinsky model should approximate SFS stress in 3D turbulence relatively well, because the spectral eddy viscosity coefficient corresponding to Gaussian and box filters is almost constant on a wide range of scales (see Leslie & Quarini 1979; Cerutti *et al.* 2000). There is a theoretical estimate of the Smagorinsky constant ($C_S \approx 0.16$) for homogeneous isotropic turbulence with filter scale belonging to the inertial range of direct energy cascade (Meneveau & Katz 2000; Lilly 1967), and this estimate is close to values used in practice. The grid-convergent turbulence statistics can be achieved with the use of the Smagorinsky model by fixing filter width ($\overline{\Delta}$) and C_S, and then refining the computational grid (see Sarwar *et al.* 2017). In 2D turbulence, the SFS stress energy transfer spectrum corresponding to a Gaussian filter has more complex structure, and thus more accurate SFS models are needed, as will be shown below.

In 3D turbulence, the optimal value of the Smagorinsky constant was found to depend on the resolved flow, i.e., on the presence of the strong mean shear, on the mesh resolution and

on the distance to a wall in wall-bounded problems (Sagaut 2006). Germano *et al.* (1991) proposed the dynamic procedure, which estimates the Smagorinsky constant locally based on the resolved flow without the need for empirical adjusting of C_S. This procedure has the following useful properties: it gives values close to the theoretical estimate ($C_S \approx 0.16$) for homogeneous turbulence (Meneveau & Lund 1997), gives correct asymptotic behaviour in the viscous sublayer (Germano *et al.* 1991), gives zero C_S for laminar flows and is thus beneficial in laminar-turbulent transition (Vreman *et al.* 1997; Vreman 2004), and it is at least weakly sensitive to the Reynolds number (Meneveau & Lund 1997). The latter property means that the Smagorinsky constant approaches zero as the mesh-Reynolds number decreases, ($\lim_{Re_\Delta \to 0} C_S = 0$), i.e., the dynamic procedure should be sensitive to the shape of the energy spectrum at filter scale: it reduces the Smagorinsky constant if the solution is too damped (for example, due to dissipation introduced by the numerical scheme) and increases the Smagorinsky constant if the solution is too noisy.

Whether the dynamic procedure can be useful for 2D turbulence remains unclear. According to the authors' knowledge, the dynamic procedure (with local eddy viscosity coefficient) was inserted into the ocean model based on primitive equations only once (Bachman *et al.* 2017), and no substantial improvements over closure with the prescribed coefficient was found. Examples of the application of the dynamic model in QG equations can be found in papers (San 2014; Maulik & San 2016, 2017*b*,*d*,*a*). Although some results are satisfactory, particularly when the Reynolds number is low, a specific numerical discretization, discrete filter, filter width ratio and viscosity kernel are chosen. Nevertheless, numerical noise often arises in the smallest resolved scales. Based on our experience with dynamic models, we suppose that noisy solutions more frequently occur in 2D turbulence, compared to 3D turbulence, possibly due to a number of reasons: a large discrepancy between SFS stress and the eddy viscosity model, a stronger sensitivity to numerical effects (i.e., larger FGRs are needed to suppress numerical noise), and improper response to the growth of energy in the smallest resolved scales. In particular, dynamic model in 2D turbulence predicts slightly larger C_S when reducing the Reynolds number (see Maulik & San 2017*d*), in contrast to 3D turbulence. In this work, we aim to clarify the first two points. The importance of local adjustment of the eddy viscosity in 2D turbulence (near boundary, in strong mean shears, in quasi-laminar flows) remains to be investigated in further studies.

Cascades of energy and enstrophy in homogeneous two-dimensional turbulence are opposite in direction (Kraichnan 1967; Leith 1968; Batchelor 1969), and thus both dissipation and backscatter of energy due to SFS stress are important to correctly simulate resolved scales (Perezhogin *et al.* 2017, 2019). Decomposition of SFS stress into dissipation and backscatter parts can be implemented at least in four ways. First, the most common approach is the decomposition in physical space, i.e., by the sign of $-\tau_{ij}\overline{S}_{ij}$. Second, the decomposition in Fourier space is possible, i.e., by the sign of $\mathrm{Re}((\tau_{ij})^*_{\boldsymbol{k}}(\overline{S}_{ij})_{\boldsymbol{k}})$, where $(\cdot)_{\boldsymbol{k}}$ stands for the Fourier transform and $*$ for the complex conjugate. Third, "stochastic backscatter" can be computed by considering the particular tendency in the EDQNM equations (Leslie & Quarini 1979). Fourth, the models for dissipation and backscatter can be proposed, and their free parameters are tuned to approximate full SFS stress. An example of such an SFS model is the combination of bilaplacian and Laplacian operators: $-\frac{\partial \sigma_j}{\partial x_j} \approx -\nu_4 \nabla^4 \overline{\omega} + \nu_2 \nabla^2 \overline{\omega}$, $\nu_4 > 0, \nu_2 \leqslant 0$, see Jansen & Held (2014).

In 2D turbulence, SFS energy and enstrophy fluxes in physical space ($\Pi_E = -\tau_{ij}\overline{S}_{ij}$ and $\Pi_Z = -\sigma_j \frac{\partial \overline{\omega}}{\partial x_j}$, respectively) could be of either sign, and only a small average value defines the direction of the corresponding cascade across a filter scale (see Rivera *et al.* 2003; Chen *et al.* 2006, 2003). The key properties of the SFS stress for the Gaussian filter can be obtained

by considering the following expansion (Leonard 1997)

$$\sigma_j \approx \sigma_j^{\mathrm{NGM}} = \frac{\overline{\Delta}^2}{12}\frac{\partial \overline{u}_j}{\partial x_k}\frac{\partial \overline{\omega}}{\partial x_k},\ \tau_{ij} \approx \tau_{ij}^{\mathrm{NGM}} = \frac{\overline{\Delta}^2}{12}\frac{\partial \overline{u}_i}{\partial x_k}\frac{\partial \overline{u}_j}{\partial x_k}, \tag{1.10}$$

with the residual error of $O(\overline{\Delta}^4)$. Stresses σ_j^{NGM} and τ_{ij}^{NGM} correspond to the same subfilter model (NGM, Clark *et al.* 1979), but in different model variables, and they are related to each other by the curl (Chen *et al.* 2006). This subfilter model correlates highly with SFS stress (up to 99%), accurately predicts negative, positive and average values of enstrophy flux and gives zero energy flux pointwise in space, $-\tau_{ij}^{\mathrm{NGM}}\overline{S}_{ij} = 0$ (see Chen *et al.* 2003, 2006; Nadiga 2008). The latter property of SFS stress,

$$\Pi_E \approx -\tau_{ij}^{\mathrm{NGM}}\overline{S}_{ij} = 0, \tag{1.11}$$

is often utilized in "energetically consistent" KEB parameterizations. In these parameterizations, approximate local equilibration of energy fluxes corresponding to eddy viscosity and backscatter models is achieved either by introducing subgrid kinetic energy (Jansen *et al.* 2015) or by choosing the variance of the stochastic backscatter model to be proportional to the local energy dissipation (Berner *et al.* 2009). Let $T(k)$ be an energy transfer spectrum corresponding to the NGM model. Then, dissipation of enstrophy and conservation of energy imply, respectively:

$$\int T(k)k^2 dk < 0 \text{ and } \int T(k)dk = 0. \tag{1.12}$$

It follows from the first relation that there is a region of energy dissipation ($T(k) < 0$), and then, the second relation gives another region of energy generation ($T(k) > 0$). Thus, often reported kinetic energy backscatter in large scales in Fourier space for 2D turbulence (Thuburn *et al.* 2014; Frederiksen *et al.* 2003; Perezhogin *et al.* 2019; Kraichnan 1976) is connected to the following property of SFS stress: $\Pi_E \approx 0$.

Although the property of energy conservation by the SFS model is a good approximation for statistically-steady turbulent flows, like 2D turbulence forced on a spatial scale larger than the base filter width, in decaying 2D turbulence the energy of the filtered DNS solution grows (Bouchet 2003). In this work, by considering the equation for subfilter energy, we derive an approximate relation between SFS energy and enstrophy fluxes in decaying 2D turbulence at a high Reynolds number:

$$\langle \Pi_E \rangle = -\frac{\overline{\Delta}^2}{12}\langle \Pi_Z \rangle, \tag{1.13}$$

where $\langle\cdot\rangle$ denotes spatial averaging. Energy and esntrophy fluxes are oppositely directed on average, and anti-correlation is found even for pointwise fluxes: $\Pi_E \sim -\Pi_Z$. The relation (1.13) clearly shows that to correctly predict growth of resolved energy, the SFS model should at least correctly describe dissipation of enstrophy corresponding to a given filter width.

Let us underline the complicated interplay between energy and enstrophy fluxes in 2D turbulence. First, accurate simulation of dissipation and backscatter of enstrophy (as the NGM model does) does not guarantee the correct reproduction of upscale transfer of energy from unresolved to resolved scales in decaying turbulence. Second, although NGM approximation is orthogonal to the strain-rate tensor, it still plays a substantial role in dynamics: it redistributes energy from smallest to largest resolved scales and dissipates enstrophy. Thus, the leading order impact of SFS stress on the resolved energy is carried out by the divergence of resolved energy space transport, i.e., $-\dfrac{\partial}{\partial x_j}\left(\overline{u}_i\tau_{ij}\right)$. Third, pointwise

energy and enstrophy fluxes are often opposite in direction, and this behaviour cannot be captured by a simple eddy viscosity model.

As follows from a review given above, it is difficult to construct a model for the full SFS stress in 2D turbulence, which correctly simulates energy and enstrophy exchange with subfilter scales. Thus, we aim to decompose the SFS stress into parts that can be clearly attributed to backscatter of energy and dissipation of enstrophy. Consider the Germano decomposition of SFS stress (Germano 1986; Nadiga 2008)

$$\sigma_j = \underbrace{\overline{\overline{u}_j\overline{\omega}} - \overline{\overline{u}}_j\overline{\overline{\omega}}}_{\text{Leonard stress}} + \underbrace{\overline{\overline{u}_j\omega'} + \overline{u'_j\overline{\omega}} - \overline{\overline{u}}_j\overline{\omega'} - \overline{u'_j}\,\overline{\overline{\omega}}}_{\text{cross stress}} + \underbrace{\overline{u'_j\omega'} - \overline{u'_j}\,\overline{\omega'}}_{\text{Reynolds stress}}, \tag{1.14}$$

where prime denotes subfilter fields, $\omega' = \omega - \overline{\omega}$ and $u'_j = u_j - \overline{u}_j$. Leonard stress can be computed directly from filtered fields and need not to be approximated. We show in a priori analysis that cross stress provides enstrophy dissipation and that its enstrophy transfer spectrum can be approximated by bilaplacian eddy viscosity. Reynolds stress predominantly injects energy into large scales in Fourier space. This finding is different from 3D homogeneous turbulence, where Reynolds stress dissipates energy (Schilling & Zhou 2002; Hughes *et al.* 2004). In 2D turbulence, the decomposition of SFS stress into a series of contributions of subfilter scales shows that upscale kinetic energy flux is formed by the smallest eddies (Chen *et al.* 2006). Thus, our finding is consistent with the physics of the inverse energy cascade.

This paper is organized as follows. In section 2, we describe energy and enstrophy transfer in a priori analysis. In section 3, we propose a set of LES models with explicit filtering, ranging from the simplest approach (dynamic Smagorinsky model) to the new three-component model that approximates each part in Germano decomposition (1.14). The cross term is approximated with the Smagorinsky bilaplacian viscosity, and Reynolds is approximated with a deconvolution procedure. Free parameters of the parameterization are found using a dynamic procedure and an energy-enstrophy balance equation (1.13). In section 4, we investigate the ability of LES models to simulate filtered DNS solution and SFS energy and enstrophy transfers.

2. A priori analysis of SFS stress

An experiment of 2D decaying turbulence is analogous to the work Maulik & San (2017*a*). Equations (1.1) and (1.2) are solved in a doubly-periodic domain of size $2\pi \times 2\pi$. An initial condition is a random divergence-free flow field with the following kinetic energy density (per unit wavenumber k and unit area):

$$E(k) = Ak^4 \exp\left(-(k/k_p)^2\right), \; A = \frac{4k_p^{-5}}{3\sqrt{\pi}}, \tag{2.1}$$

where $k = \sqrt{k_1^2 + k_2^2}$; $k_1, k_2 \in \mathbb{Z}$ – components of wavevector $\boldsymbol{k} = (k_1, k_2)$, $k_p = 10$. Constant A gives the following initial energy per unit area:

$$\langle \frac{1}{2} u_i u_i \rangle = \int E(k)dk = \frac{1}{2}, \tag{2.2}$$

where $\langle\cdot\rangle$ – spatial averaging. This experiment is described in at least two papers (Maulik & San 2017*a*,*d*), where different values of A are given. We used the value from the first paper.

The numerical integration is performed until dimensionless time $t = 10$. All statistical characteristics of the turbulence presented are averaged over an ensemble of 50 realizations

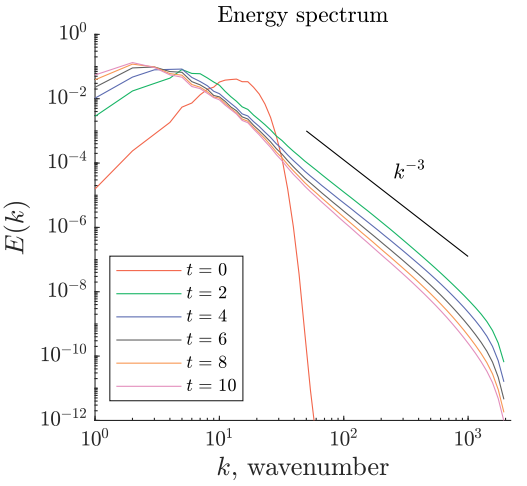

Figure 1: Ensemble-averaged (50 realizations) energy spectrum in DNS at 4096^2 resolution and $Re = 512000$.

of the initial random field. Computations are carried out in hydrodynamic code of Mortikov *et al.* (2019), particularly in its modification for 2D hydrodynamics (Perezhogin *et al.* 2017). The numerical mesh is uniform. The Reynolds number ($Re = 512000$) is 4 times larger, and the resolution of DNS (4096×4096) is twice that in work Maulik & San (2017*a*). The second-order Arakawa scheme with two invariants (energy and enstrophy, Arakawa 1997; Maulik & San 2017*d*)) is used for numerical discretization of the vorticity advection term. The relation (1.4) between streamfunction and velocity is discretized on the Arakawa C grid (Arakawa & Lamb 1977) using second-order finite differences. The Fast Fourier transform library FFTW (Frigo & Johnson 1998) is used for solving the Poisson equation (1.2), where the Laplace operator is discretized with second-order finite differences. A three-stage Runge-Kutta (RK3) scheme (Skamarock *et al.* 2008) is used for time integration, with time step Δt satisfying stability criterion $\mathrm{CFL} = \Delta t \max_j(|u_j|)/\Delta_g < 0.7$, Δ_g – grid step. Decay of an initial kinetic energy spectrum is shown in figure 1.

The base filter (denoted by $\overline{(\cdot)}$) is Gaussian and applied in Fourier space, its transfer function is given by (Sagaut 2006):

$$\widetilde{G}(k_1, k_2, \overline{\Delta}) = \exp\left(-\frac{\overline{\Delta}^2(k_1^2 + k_2^2)}{24}\right), \tag{2.3}$$

where $\overline{\Delta}$ – filter width.

2.1. *Total energy flux*

We first derive and test the relation between energy and enstrophy fluxes (1.13). Let e be a subfilter energy defined by (Germano 1992; Ghosal *et al.* 1995):

$$e = \frac{1}{2}\left(\overline{u_i u_i} - \overline{u}_i \overline{u}_i\right) = \frac{1}{2}\tau_{ii}. \tag{2.4}$$

We estimate e utilizing NGM approximation of SFS stress:

$$e \approx \frac{1}{2}\tau_{ii}^{NGM} = \frac{\overline{\Delta}^2}{24}\frac{\partial \overline{u}_i}{\partial x_j}\frac{\partial \overline{u}_i}{\partial x_j}. \tag{2.5}$$

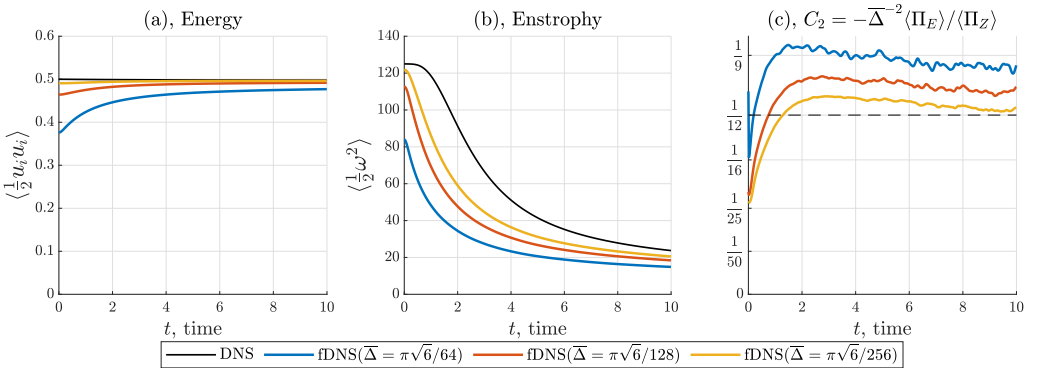

Figure 2: (a) Energy and (b) enstrophy of the DNS and filtered DNS (fDNS), (c) estimation of constant C_2 in (2.9) based on the fDNS data. Filter width is given in the legend.

Similar estimation was proposed, for example, in Pomraning & Rutland (2002) (see their equation 71) and Verstappen (2011) (page 100). Decomposing velocity gradient tensor $\frac{\partial\overline{u}_i}{\partial x_j}$ into symmetric $\overline{S}_{ij}$ and antisymmetric $\overline{\Omega}_{ij}$ parts, one obtains $\frac{\partial\overline{u}_i}{\partial x_j}\frac{\partial\overline{u}_i}{\partial x_j} = \overline{S}_{ij}\overline{S}_{ij} + \overline{\Omega}_{ij}\overline{\Omega}_{ij} = |\overline{S}|^2/2 + \overline{\omega}^2/2$. Finally, as $\langle|\overline{S}|^2\rangle = \langle\overline{\omega}^2\rangle$ (Buxton *et al.* 2011), we give the following estimation for subfilter energy based on the resolved enstrophy ($Z = \overline{\omega}^2/2$):

$$\langle e\rangle = \frac{\overline{\Delta}^2}{12}\langle Z\rangle. \tag{2.6}$$

In the absence of energy sources and in the limit of a very high Reynolds number (i.e., dissipation of energy by molecular viscosity is negligible), total subfilter energy can only change due to the interaction with resolved flow, i.e.:

$$\frac{d}{dt}\langle e\rangle = \langle\Pi_E\rangle, \tag{2.7}$$

where $\Pi_E = -\tau_{ij}\overline{S}_{ij}$ is an energy flux from resolved to subfilter scales. Under the same conditions, resolved enstrophy can be lost only to the subfilter scales, i.e.:

$$\frac{d}{dt}\langle Z\rangle = -\langle\Pi_Z\rangle, \tag{2.8}$$

where $\Pi_Z = -\sigma_j\frac{\partial\overline{\omega}}{\partial x_j}$ is an enstrophy flux from resolved to subfilter scales. Combining equations (2.6), (2.7) and (2.8), we arrive at the energy-enstrophy balance equation:

$$\langle\Pi_E\rangle = -C_2\overline{\Delta}^2\langle\Pi_Z\rangle, \tag{2.9}$$

where $C_2 = \frac{1}{12}$ according to presented analytical derivation.

Figure 2 shows that for various filter widths ($\overline{\Delta} = \pi\sqrt{6}/64,\ \pi\sqrt{6}/128,\ \pi\sqrt{6}/256$) resolved energy grows and resolved enstrophy decays. Enstrophy decay at a late time is not described by the Batchelor (1969) law $\langle\frac{1}{2}\omega^2\rangle \sim t^{-2}$ either in DNS or in filtered DNS data, but the law is closer to $t^{-0.8}$ (not shown) as found in Chasnov (1997). Averaged energy and enstrophy fluxes are directed oppositely, and analytical estimate $C_2 = \frac{1}{12}$ gives a lower bound on the energy flux in the developed turbulence regime ($t > 1$); see figure 2(c). This value will be used in a posteriori experiments. Note that fluxes Π_E and Π_Z are also anti-correlated pointwise in physical space at the -80% level. As this property will not be used further in construction of LES models, we do not provide an additional figure.

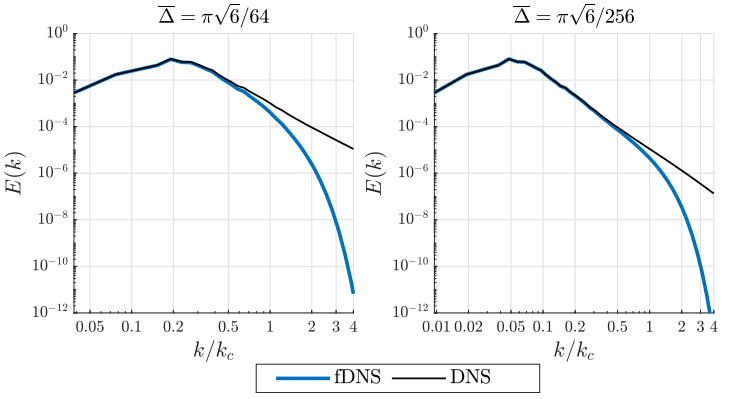

Figure 3: Energy spectrum in DNS and filtered DNS at $t = 2$, $k_c = \pi/\overline{\Delta}$ – filter wavenumber.

2.2. *Transfer spectra for Germano decomposition*

An amount of energy and enstrophy exchange with subfilter scales, $\langle \Pi_E \rangle$ and $\langle \Pi_Z \rangle$, depends on the time moment. For three filter widths presented, these fluxes reach their maximum values until $t = 1$, and then the exchange steadily decreases. We analyse transfer spectra at $t = 2$ when the energy spectrum is already well developed, but the exchange is still substantial. Energy spectra of DNS and filtered DNS are given in figure 3.

Enstrophy and energy transfer spectra integrated over a circle for SFS stress σ_j are defined as follows, respectively:

$$T_Z(k) = \sum_{|\boldsymbol{k}|\in[k,k+1)} \mathrm{Re}\left(-\left(\frac{\partial \sigma_j}{\partial x_j}\right)^*_{\boldsymbol{k}} (\overline{\omega})_{\boldsymbol{k}}\right), \tag{2.10}$$

$$T_E(k) = \sum_{|\boldsymbol{k}|\in[k,k+1)} \mathrm{Re}\left(\left(\frac{\partial \sigma_j}{\partial x_j}\right)^*_{\boldsymbol{k}} (\overline{\psi})_{\boldsymbol{k}}\right), \tag{2.11}$$

where $(\cdot)_{\boldsymbol{k}}$ stands for Fourier transform, $*$ for complex conjugate. The Fourier transform is normalized to give:

$$\int T_Z(k)\mathrm{d}k = -\langle \Pi_Z \rangle, \int T_E(k)\mathrm{d}k = -\langle \Pi_E \rangle. \tag{2.12}$$

Note that in the absence of finite differencing errors the following relation holds $T_Z(k) = T_E(k)k^2$.

Figures 4 and 5 show power and transfer spectra for SFS stress and its components according to the Germano decomposition (1.14). The power law $k^{2.46}$ given for power spectrum corresponds to $k^{0.46}$ in momentum tendency, and it was reported in Berner *et al.* (2009).

We give the key properties of the full SFS stress (black line):

- The major part of the enstrophy transfer spectrum is the enstrophy dissipation (i.e., $T_Z(k) < 0$).
- Approximately 50% of the enstrophy dissipation corresponds to subfilter scales in the wavenumber range $1 < k/k_c < 3$.
- Energy transfer spectrum consists of small-scale dissipation ($T_E(k) < 0$) and large-scale backscatter ($T_E(k) > 0$).
- Energy backscatter occurs at wavenumbers, where SFS power spectrum is low.

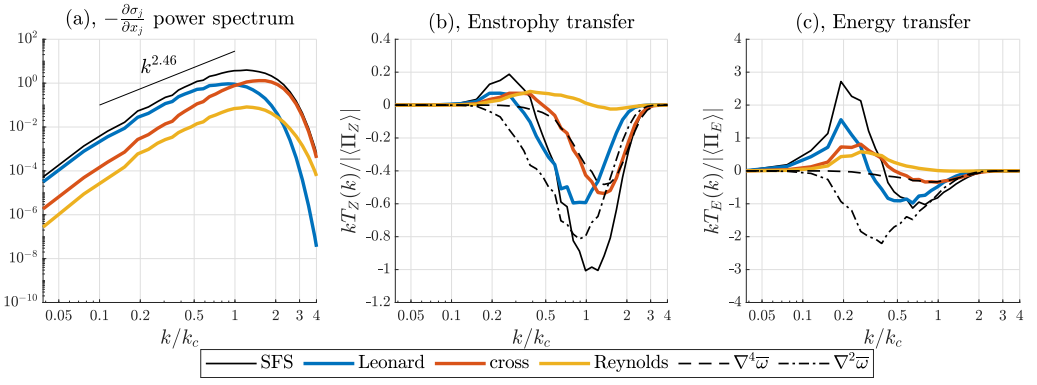

Figure 4: A priori results averaged over the ensemble, $\overline{\Delta} = \pi\sqrt{6}/64$ and $t = 2$, $k_c = \pi/\overline{\Delta}$ – filter wavenumber. (a) power spectrum, (b) enstrophy transfer spectrum and (c) energy transfer spectrum for full SFS stress, and its components (Leonard, cross, Reynolds); $\nabla^2\overline{\omega}$ – approximation of SFS stress by Laplacian operator, $\nabla^4\overline{\omega}$ – approximation of cross stress by bilaplacian operator.

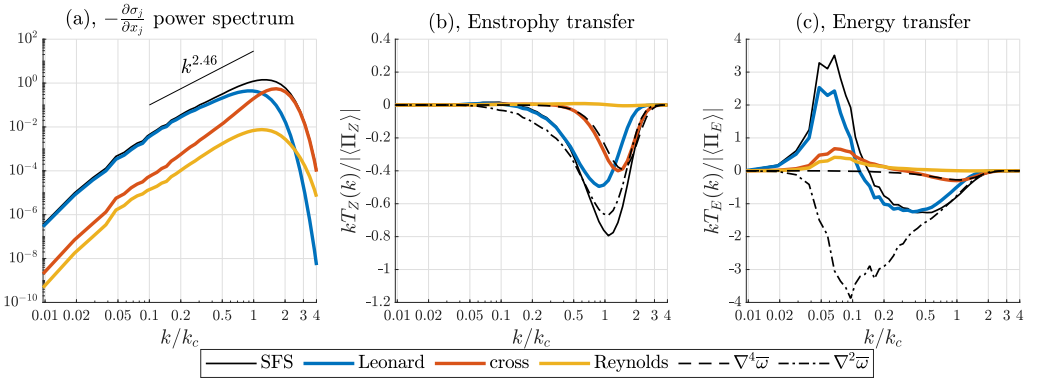

Figure 5: The same as figure 4, but $\overline{\Delta} = \pi\sqrt{6}/256$.

- Laplacian eddy viscosity ($-\frac{\partial \sigma_j}{\partial x_j} \approx \nu\nabla^2\overline{\omega}$) approximates the enstrophy transfer spectrum relatively well, but does not predict the energy transfer spectrum in a wide range of scales ($k/k_c < 0.5$).

The major properties of SFS stress components:

- Enstrophy dissipation is represented by Leonard and cross stresses.
- The enstrophy dissipation corresponding to cross stress has small spatial scale and can be approximated by bilaplacian eddy viscosity ($-\frac{\partial \sigma_j}{\partial x_j} \approx -\nu\nabla^4\overline{\omega}$).
- Cross stress contributes most into SFS stress power spectrum in subfilter scales. The applicability of the eddy viscosity approximation for cross stress will be discussed in a posteriori experiments.
- All three components (Leonard, cross, Reynolds) of SFS stress contribute to the energy backscatter on large scales.
- Reynolds stress almost purely corresponds to energy backscatter in Fourier space: it gives energy generation on large scales, while contribution to enstrophy transfer on small scales is negligible. This property is in contrast to a usual model of energy backscatter –

Laplacian viscosity with a negative coefficient, which substantially changes the enstrophy budget.

• The Reynolds stress is composed of unresolved fields (u'_j, ω') and therefore it is often replaced by stochastic backscatter models (Grooms *et al.* 2015; Schumann 1995). These models simulate power spectrum of the Reynolds stress, which is assumed to be universal in k/k_c units (Leslie & Quarini 1979), and provides energy input near the filter scale. However, we found that the correlation of Reynolds stress with the resolved flow is that the energy is injected on large scales, approximately corresponding to the peak in the energy spectrum, and thus spatial scale of energy backscatter is determined by some integral length scale of turbulent flow and cannot be universal in k/k_c units.

Kraichnan (1976) predicted that spectral eddy viscosity coefficient associated with the SGS stress approaches a constant negative value on large scales. This result was later verified in numerical simulations (see, for example, Frederiksen & Kepert 2006). If there was a region of constant spectral eddy viscosity, the negative viscosity backscatter model ($-\frac{\partial \sigma_j}{\partial x_j} \approx \nu \nabla^2 \overline{\omega}, \nu \leqslant 0$) could correctly reproduce the SGS energy transfer spectrum on a large scale. We have not found a region of strictly constant spectral eddy viscosity (not shown). Possibly, existence of this region depends on the configuration of inertial intervals, filter shape and presence of external forcing. In what follows, we will assume that the backscatter parameterization should have an energy transfer spectrum similar in shape to the shape of the Reynolds stress.

Based on the a priori analysis, we propose the following approach to construct the SFS model. Leonard stress can be computed directly, and enstrophy dissipation associated with cross stress can be approximated by the bilaplacian eddy viscosity model. A lack of kinetic energy backscatter on large scales is proposed to compensate by the simplest approximation to Reynolds stress: an approximate deconvolution (AD) procedure of lowest order. See next section for details.

3. LES models

In this section, we describe four SFS models with explicit filtering. The eddy viscosity coefficient is estimated using a dynamic procedure in a least squares formulation with horizontal averaging, see section 3.1 in Ghosal *et al.* (1995). Contrary to 3D turbulence, the dynamic procedure is applied in vorticity variables, because SFS stress in velocity variables satisfies $\langle -\tau_{ij} \overline{S}_{ij} \rangle \approx 0$, and thus the predicted eddy viscosity may be close to zero and with any sign. Note that local constraining of eddy viscosity to be positive (clipping) in velocity formulation of dynamic model can give satisfactory results for quasi-2D fluids (Bachman *et al.* 2017; Pawar *et al.* 2020; Guan *et al.* 2021). There are various approaches to choose the eddy viscosity kernel, i.e., constant, Smagorinsky or Leith eddy viscosities; see Bachman *et al.* (2017); Maulik & San (2017*d*). Some authors claim that a particular viscosity kernel can be more scale-selective (Pearson *et al.* 2017), while the others suggest that the eddy viscosity kernel cannot change the scale-selectivity property (Griffies & Hallberg 2000). We have checked that the type of viscosity kernel (constant, Smagorinsky, Leith) for the Laplacian operator in a priori analysis does not influence the shape of the corresponding enstrophy transfer spectrum, and thus we present here results only for the Smagorinsky eddy viscosity kernel.

Germano *et al.* (1991) identity in vorticity variables reads

$$l_j = \Sigma_j - \widehat{\sigma}_j, \tag{3.1}$$

where $\widehat{(\cdot)}$ denotes test filter of width $\widehat{\Delta}$, $l_j = \widehat{\overline{u_j}\,\overline{\omega}} - \widehat{\overline{u}}_j\widehat{\overline{\omega}}$ – resolved subfilter stress, σ_j and $\Sigma_j = \widehat{\overline{u_j}\,\overline{\omega}} - \widehat{\overline{u}}_j\widehat{\overline{\omega}}$ – subfilter stresses at $\overline{\Delta}$ and $\widehat{\overline{\Delta}}$ levels, respectively. In explicit filtering approach a combination of filters $\widehat{\overline{(\cdot)}}$ should be similar to the base filter $\overline{(\cdot)}$, see Winckelmans *et al.* (2001). This restricts us to choose the Gaussian test filter (discrete filter will be given below), and then width of filter $\widehat{\overline{(\cdot)}}$ is $\widehat{\overline{\Delta}} = \sqrt{\overline{\Delta}^2 + \widehat{\Delta}^2}$ (Germano 1992). Because l_j can be computed directly, replacing subfilter stresses σ_j and Σ_j by an SFS model allows the estimation of a Smagorinsky constant from the Germano identity. The following stresses will be used as components of SFS models:

$$m_j^{\mathrm{lap}}[\overline{\Delta}] = -\overline{\Delta}^2|\overline{S}|\frac{\partial\overline{\omega}}{\partial x_j}, \tag{3.2}$$

$$m_j^{\mathrm{bilap}}[\overline{\Delta}] = \overline{\Delta}^4|\overline{S}|\frac{\partial(\nabla^2\overline{\omega})}{\partial x_j}, \tag{3.3}$$

$$m_j^{\mathrm{ssm}}[\overline{\Delta}] = \overline{\overline{u}_j\overline{\omega}} - \overline{\overline{u}}_j\overline{\overline{\omega}}, \tag{3.4}$$

$$m_j^{\mathrm{keb}}[\overline{\Delta}] = \overline{\overline{u_j'}\,\overline{\omega'}} - \overline{\overline{u_j'}}\,\overline{\overline{\omega'}}. \tag{3.5}$$

Here a notation $[\overline{\Delta}]$ means that the filter appearing anywhere in the flux has a prescribed width $\overline{\Delta}$. Flux m_j^{keb} is a lowest-order AD approximation of Reynolds stress, where $\overline{u_j'} = \overline{u_j} - \overline{\overline{u_j}}$ and $\overline{\omega'} = \overline{\omega} - \overline{\overline{\omega}}$. The connection to the AD procedure is clear if we consider a Van Cittert iteration $\omega \approx 2\overline{\omega} - \overline{\overline{\omega}}$ (Layton & Rebholz 2012), then $\omega' = \omega - \overline{\omega} \approx \overline{\omega'}$. A similar approximation of the Reynolds stress (but in the form $\overline{u_i'u_j'} \approx \overline{u_i'}\,\overline{u_j'}$) for the first time was proposed by Bardina *et al.* (1980), which was necessary to derive the SSM model. Later various other approximations were studied; see Horiuti (1997) for details.

The four stresses presented can be calculated explicitly given a filtered solution $(\overline{\omega}, \overline{u}_j)$ on $\overline{\Delta}$ and $\widehat{\overline{\Delta}}$ levels. Four dynamic SFS models for σ_j are given below:

- Laplacian model (`lap`):

$$\sigma_j^m = C_S^2 m_j^{\mathrm{lap}}[\overline{\Delta}], \tag{3.6}$$

where $C_S^2 = \frac{\langle l_j\alpha_j\rangle}{\langle\alpha_j\alpha_j\rangle}$ and $\alpha_j = m_j^{\mathrm{lap}}[\widehat{\overline{\Delta}}] - \widehat{m_j^{\mathrm{lap}}[\overline{\Delta}]}$.

- Bilaplacian model (`bilap`):

$$\sigma_j^m = C_S^4 m_j^{\mathrm{bilap}}[\overline{\Delta}], \tag{3.7}$$

where $C_S^4 = \frac{\langle l_j\alpha_j\rangle}{\langle\alpha_j\alpha_j\rangle}$ and $\alpha_j = m_j^{\mathrm{bilap}}[\widehat{\overline{\Delta}}] - \widehat{m_j^{\mathrm{bilap}}[\overline{\Delta}]}$.

- Mixed model (`ssm`+`bilap`):

$$\sigma_j^m = m_j^{\mathrm{ssm}}[\overline{\Delta}] + C_S^4 m_j^{\mathrm{bilap}}[\overline{\Delta}], \tag{3.8}$$

where $C_S^4 = \frac{\langle(l_j - h_j)\alpha_j\rangle}{\langle\alpha_j\alpha_j\rangle}$, $h_j = m_j^{\mathrm{ssm}}[\widehat{\overline{\Delta}}] - \widehat{m_j^{\mathrm{ssm}}[\overline{\Delta}]}$ and $\alpha_j = m_j^{\mathrm{bilap}}[\widehat{\overline{\Delta}}] - \widehat{m_j^{\mathrm{bilap}}[\overline{\Delta}]}$.

- Three-component model (`ssm`+`bilap`+`keb`):

$$\sigma_j^m = m_j^{\mathrm{ssm}}[\overline{\Delta}] + C_S^4 m_j^{\mathrm{bilap}}[\overline{\Delta}] + C_R m_j^{\mathrm{keb}}[\overline{\Delta}], \tag{3.9}$$

where $C_S^4 = \frac{\langle(l_j - h_j)\alpha_j\rangle}{\langle\alpha_j\alpha_j\rangle}$, $h_j = m_j^{\mathrm{ssm}}[\widehat{\overline{\Delta}}] - \widehat{m_j^{\mathrm{ssm}}[\overline{\Delta}]}$ and $\alpha_j = m_j^{\mathrm{bilap}}[\widehat{\overline{\Delta}}] - \widehat{m_j^{\mathrm{bilap}}[\overline{\Delta}]}$. Energy-

enstrophy balance equation (2.9) gives an equation for finding C_R: $\langle \sigma_j \frac{\partial \overline{\psi}}{\partial x_j} \rangle = C_2 \overline{\Delta}^2 \langle \sigma_j \frac{\partial \overline{\omega}}{\partial x_j} \rangle$. Solving for C_R we have

$$C_R = -\frac{\langle (m_j^{\mathrm{ssm}}[\overline{\Delta}] + C_S^4 m_j^{\mathrm{bilap}}[\overline{\Delta}])\beta_j \rangle}{\langle m_j^{\mathrm{keb}}[\overline{\Delta}]\beta_j \rangle}, \tag{3.10}$$

where $\beta_j = \frac{\partial \overline{\psi}}{\partial x_j} - C_2 \overline{\Delta}^2 \frac{\partial \overline{\omega}}{\partial x_j}$, $C_2 = \frac{1}{12}$.

The LES models presented do not contain a grid step and should give grid-convergent turbulence statistics. The proposed model of kinetic energy backscatter (stress $C_R m_j^{\mathrm{keb}}$) has almost no effect on the integral enstrophy balance, as it is clear from a priori experiments and will be additionally shown in a posteriori experiments. Its usage does not require an additional tuning of the enstrophy dissipation model, and this is an important property from the practical point of view. Indeed, kinetic energy backscatter and eddy viscosity models designed for quasi-2D turbulence are usually developed independently. However, m_j^{keb} highly correlates with SFS stress (at the level 40 – 60%) and significantly changes pointwise enstrophy balance. Inclusion of this stress into the Germano identity leads to underestimation of the Smagorinsky constant. In the latter LES model, this stress is eliminated from the Germano identity, and we found that this approach yields more robust numerical results. Usually, if some simplification is made in the Germano identity, then it is necessary to check that this simplification does not lead to large error in the identity, and this will be discussed in a posteriori experiments.

The numerical schemes used in the LES models are the same as in the DNS model and they are described in the section 2. SFS models are discretized with second-order numerical schemes. Base and test filters in LES models are Gaussian and applied in Fourier space if $\epsilon = \overline{\Delta}/\Delta_g > \sqrt{6}$, where Δ_g – grid step. Otherwise, $\epsilon \leqslant \sqrt{6}$, we use second-order approximation to Gaussian filter (Sagaut & Grohens 1999). One-dimensional filter reads

$$\overline{\phi}_j^x = \frac{1}{24}\epsilon^2(\phi_{j+1} + \phi_{j-1}) + (1 - \frac{\epsilon^2}{12})\phi_j, \tag{3.11}$$

where j is an index of a grid node. The two-dimensional filter is a sequential application of one-dimensional filters along x_1 and x_2 directions.

Combination of filters $\widehat{\overline{(\cdot)}}$ is computed as a sequential application of base and test filters. Formula $\widehat{\overline{\Delta}} = \sqrt{\overline{\Delta}^2 + \widehat{\Delta}^2}$ can be shown to hold for discrete filters (3.11), if the definition of filter width according to Lund (1997) is applied:

$$\overline{\Delta}/\Delta_g = \sqrt{12 \sum_j j^2 W_j}, \tag{3.12}$$

where W_j – weights of discrete filter. The knowledge of $\widehat{\overline{\Delta}}$ is needed to compute the eddy viscosity model at the corresponding level.

In a posteriori experiments, the only parameter we need to set up is the base filter width $\overline{\Delta}$. Test filter has the same shape and width $\widehat{\Delta} = \overline{\Delta}$. The corresponding filter width ratio is $\widehat{\overline{\Delta}}/\overline{\Delta} = \sqrt{2}$. This choice allows us to use the same filters in SSM and backscatter models and in the Germano identity.

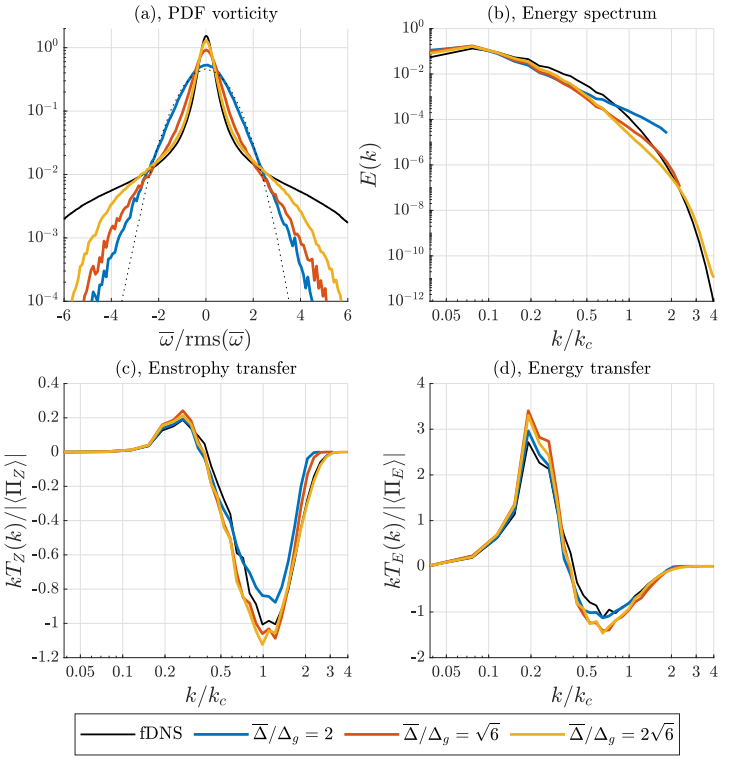

Figure 6: Grid convergence for model `ssm+bilap+keb` and comparison to a priori data. Base filter width $\overline{\Delta} = \pi\sqrt{6}/64$. Filter to grid width ratios $\overline{\Delta}/\Delta_g = 2, \sqrt{6}, 2\sqrt{6}$ and respective resolutions $104^2, 128^2, 256^2$. (a) PDF of vorticity at $t = 10$. (b) Energy spectrum at $t = 10$. (c) Enstrophy and (d) energy transfer spectra for SFS stress at $t = 2$. A dotted line shows the Gaussian PDF with dispersion equivalent to that of blue line.

4. A posteriori experiments

A posteriori experiments with LES models are carried out for the ensemble of 50 realizations. Numerical integration starts at $t = 1$, and the initial condition is prepared from DNS data as follows. We first apply a Gaussian filter of width $\overline{\Delta}$ to DNS fields, and then perform spectral truncation of wavenumbers $|k_i| > \pi/\Delta_g$, where Δ_g is a grid step of LES model.

In this section, we compare LES models in a posteriori experiments to filtered DNS data. In particular, an analysis of the statistical characteristics of the SFS stress models is given.

4.1. *Grid convergence for the three-component model*

Grid convergence of turbulence statistics in a posteriori experiments is studied for the fixed base filter width $\overline{\Delta} = \pi\sqrt{6}/64$ and varying filter to grid width ratios $\overline{\Delta}/\Delta_g = \widehat{\Delta}/\Delta_g = 2, \sqrt{6}, 2\sqrt{6}$. Corresponding grid resolutions of LES models are $104^2, 128^2, 256^2$.

Figure 6 demonstrates grid convergence of vorticity PDF, energy spectrum and transfer spectra for the three-component model (`ssm+bilap+keb`) in a posteriori experiments compared to filtered DNS data. Axes are normalized by the values of $\mathrm{rms}(\overline{\omega}) = \langle\overline{\omega}^2\rangle^{1/2}$, $\langle\Pi_Z\rangle$ and $\langle\Pi_E\rangle$ given by a priori data. The characteristics presented also converge for the rest of the three LES models. Enstrophy and energy transfer spectra are accurately reproduced by the proposed three-component model. At the coarsest resolution ($\overline{\Delta}/\Delta_g = 2$) enstrophy dissipation is becoming unresolved on the grid, although it is still close to the fDNS data; see

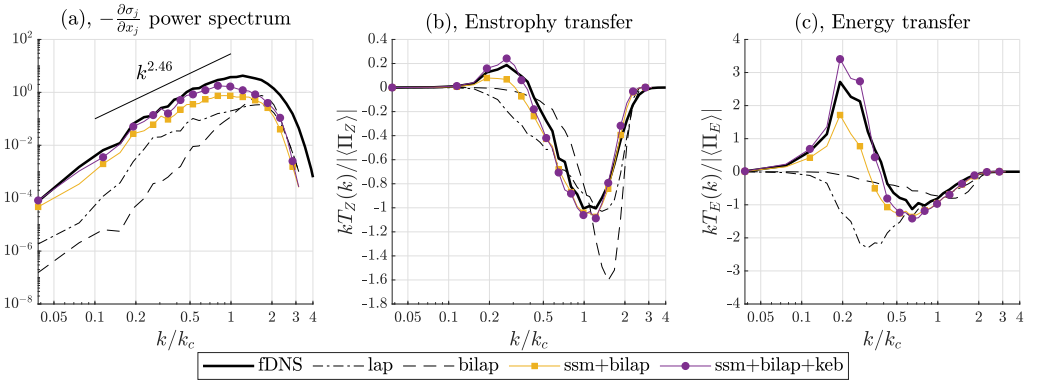

Figure 7: (a) power spectrum, (b) enstrophy and (c) energy transfer spectra for SFS models in a posteriori experiments compared to a priori data. Time moment $t = 2$, resolution 128^2, $\overline{\Delta}/\Delta_g = \sqrt{6}$.

figure 6(c). A more significant difference is seen in vorticity PDF and the energy spectrum at the end of the simulation. The vorticity field in the decaying turbulence at a late time consists of strong localized coherent vortices surrounded by weak filaments, and its PDF is significantly non-Gaussian (McWilliams 1984; Bartello & Warn 1996). Weak filaments lead to the sharp peak at $\overline{\omega} = 0$, while coherent vortices lead to the heavy tails. The vorticity PDF at resolution $\overline{\Delta}/\Delta_g = 2$ is closer to the Gaussian (see figure 6(a)), indicating that the dispersion errors of numerical schemes lead to the destruction of coherent vortices and emergence of numerical noise. The Gaussian PDF of vorticity in unforced 2D turbulence arises in underresolved simulation (Dubinkina & Frank 2007), while in forced turbulence, the Gaussian PDF often occurs (Dymnikov & Perezhogin 2018). Numerical noise is clearly seen in the energy spectrum at small scales; see figure 6(b). Numerical noise at resolution $\overline{\Delta}/\Delta_g = 2$ also arises in `ssm+bilap` and `bilap` models and is absent for `lap` model (not shown). However, for the last model, the solution is too damped; see the next section.

4.2. *Comparison of LES models*

According to the previous section, the minimal resolution required to properly resolve LES equations on the computational grid is guided by the following filter to grid width ratio $\overline{\Delta}/\Delta_g = \widehat{\Delta}/\Delta_g = \sqrt{6}$ (for second-order numerical schemes), and this ratio will be used below. LES models are tested at grid resolutions 128^2, 256^2, 512^2. Corresponding base filter widths are $\overline{\Delta} = \pi\sqrt{6}/64$, $\pi\sqrt{6}/128$, $\pi\sqrt{6}/256$.

In our setting, the filter width ratio $\widehat{\overline{\Delta}}/\overline{\Delta} = \sqrt{2}$ is considerably lower than the test filter width $\widehat{\Delta}/\Delta_g = \sqrt{6}$. In the implicit filtering approach, these parameters are assumed to be equal (i.e., $\overline{\Delta} = \Delta_g$, $\widehat{\overline{\Delta}} = \widehat{\Delta}$; see Maulik & San (2017*d*)), but in the explicit filtering approach, they must be different (Winckelmans *et al.* 2001). The filter width ratio can be considered a free parameter, and its reduction leads to an increase in eddy viscosity (San 2014).

In the SFS model `ssm+bilap+keb`, the backscatter rate is approximately 2, as a result of applying the energy-enstrophy balance equation (2.9); i.e., an amount of energy generation associated with backscatter parameterization is twice as large as the energy dissipation associated with the SSM and eddy viscosity parts of the model. In forced quasi-2D turbulence, this value is usually prescribed and chosen slightly less than 1 (Jansen & Held 2014). The typical value of the "backscatter amplitude" in a posteriori experiments with this model is $C_R \approx 20$. Although this value may seem somewhat large, we will give some arguments

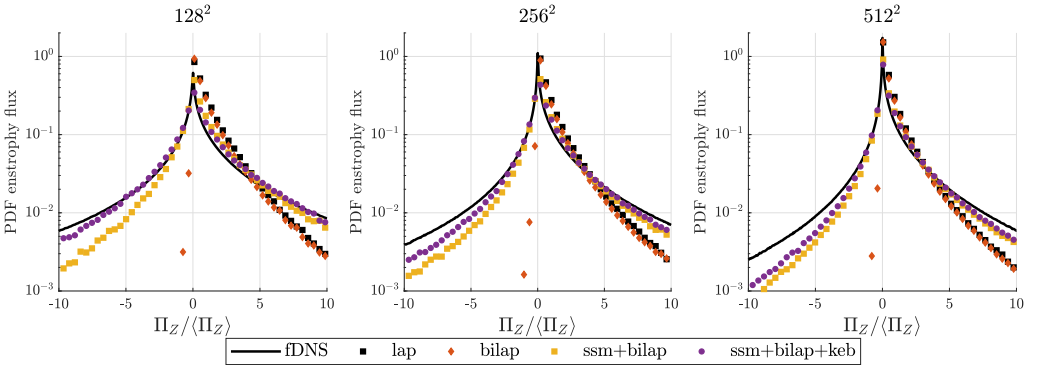

Figure 8: PDF of enstrophy dissipation in a posteriori experiments compared to a priori data. Time moment $t = 2$, $\overline{\Delta}/\Delta_g = \sqrt{6}$.

against it. First, we compared the power spectrum of the SFS model tendency $-\partial\sigma_j^m/\partial x_j$ in a posteriori experiments with the corresponding characteristic of the SFS stress, and we found that the power spectrum for all four LES models is lower than the power spectrum for SFS stress; see figure 7(a). At subfilter scales ($k/k_c > 1$), the power spectrum is considerably underestimated, because neither of the SFS models presented approximates cross stress with high accuracy. Second, an error in a priori analysis at $t = 1$ for the three-component model is ≈ 0.3 compared to ≈ 0.5 for `ssm+bilap` model and ≈ 0.9 for for `lap` and `bilap` models. The error is computed as $\langle(\partial(\sigma_j - \sigma_j^m)/\partial x_j)^2\rangle/\langle\left(\partial\sigma_j/\partial x_j\right)^2\rangle$. Third, an error in the Germano identity in a posteriori experiments for this model is less than 0.2 compared to ≈ 0.5 for `ssm+bilap` model and ≈ 0.97 for `lap` and `bilap` models. The error is computed as $\langle\varepsilon_j\varepsilon_j\rangle/\langle l_j l_j\rangle$, where $l_j = \Sigma_j^m - \widehat{\sigma_j^m} + \varepsilon_j$, and σ_j^m and Σ_j^m – a full SFS model at $\overline{\Delta}$ and $\widehat{\overline{\Delta}}$ levels, respectively, with the same parameters (C_S, C_R). Fourth, similar values for C_R have been reported in Horiuti (1997), see table III, last column.

The enstrophy and energy transfer spectra for SFS models in a posteriori experiments compared to a priori data are shown in figure 7(b,c). The Laplacian model (`lap`) describes enstrophy dissipation but introduces spurious energy dissipation on large scales. The bilaplacian model (`bilap`) is inaccurate in both characteristics. However, the bilaplacian model should probably give a good approximation to SFS stress, if the base filter is chosen to be sharper in Fourier space. The mixed model (`ssm+bilap`) correctly describes enstrophy dissipation and slightly underestimates energy backscatter on large scales. Finally, the three-component model (`ssm+bilap+keb`) compensates for the lack of energy backscatter. The backscatter parameterization almost does not influence the small scale enstrophy dissipation, and this allowed us to exclude it from the Germano identity, see section 3.

Figure 8 shows the PDF of pointwise enstrophy flux in a posteriori experiments compared to a priori data. Negative values correspond to the backscatter of enstrophy. LES models based on scale similarity assumption (`ssm+bilap+keb` and `ssm+bilap`) correctly describe enstrophy dissipation and backscatter, and they are much better in these characteristics than eddy viscosity models (`lap` and `bilap`). The proposed parameterization of kinetic energy backscatter almost does not disturb this PDF and slightly improves reproduction of pointwise enstrophy backscatter (see violet points).

The most substantial improvement for the model `ssm+bilap+keb` over the other three models is found in the prediction of resolved energy growth; see figure 9. Formula (2.9) gives us a lower bound for the backscattered energy, and we observe that the energy is slightly less than in fDNS. In accordance with the analysis of the SFS energy transfer spectrum,

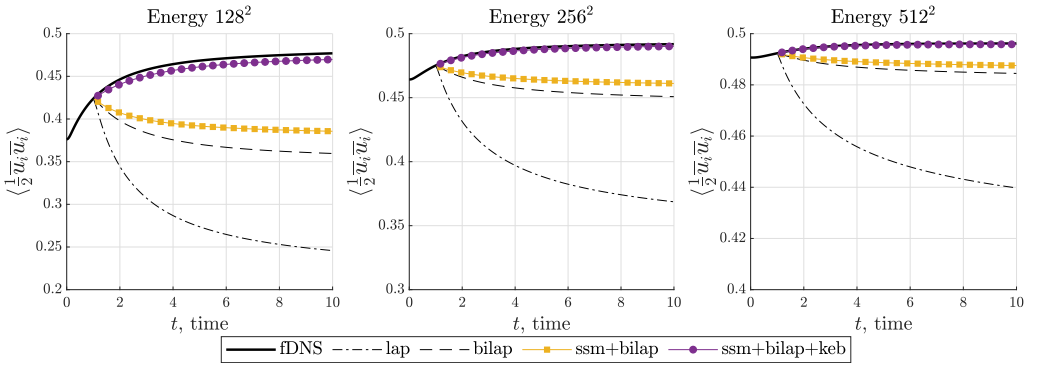

Figure 9: Energy in a posteriori experiments compared to filtered DNS data, $\overline{\Delta}/\Delta_g = \sqrt{6}$.

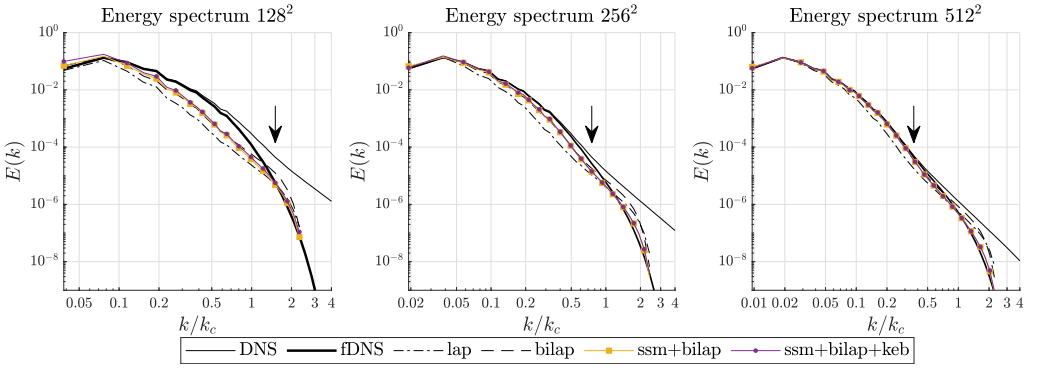

Figure 10: Energy spectrum in a posteriori experiments compared to a priori data. Time moment $t = 10$, $\overline{\Delta}/\Delta_g = \sqrt{6}$.

LES models `ssm+bilap` and `bilap` only slightly dissipate energy, while `lap` model is too dissipative.

Energy spectrum and vorticity PDF at late time $t = 10$ are shown in figures 10 and 11. The statistical characteristics presented gradually converge to fDNS data with an increase in resolution (at fixed $\overline{\Delta}/\Delta_g$) for all LES models. The slowest convergence is seen for the Laplacian model (`lap`). The energy spectrum on the smallest scales is better reproduced by models based on a scale similarity assumption (`ssm+bilap+keb` and `ssm+bilap`). The kinetic energy spectrum in DNS is not self-similar at a late time due to the joint contribution into it from coherent vortices and turbulent filaments. Coherent vortices condense on large scales and lead to the deviation of the energy spectrum from the power law. An approximate transition wavenumber between condensate and power law is indicated by an arrow. Once this scale falls within the subfilter scales ($k/k_c > 1$), all LES models underestimate the energy spectrum in middle scales; see figure 10 (128^2). In particular, instead of the complex shape of the fDNS spectrum, LES models predict a power law in this band of wavenumbers, indicating that coherent vortices are substantially weakened in a posteriori experiments; see also vorticity PDF at 128^2 resolution, figure 11. The weakening of coherent vortices is associated with the inaccuracy of the SFS models, and not with the influence of numerical errors; see the grid convergence results, figure 6(a,b). Compared to `bilap` model, reproduction of coherent vortices cannot be substantially improved either with the use of an accurate enstrophy dissipation model (`ssm+bilap`), which was shown to correctly describe the enstrophy transfer spectrum and pointwise enstrophy flux, or with the use of kinetic

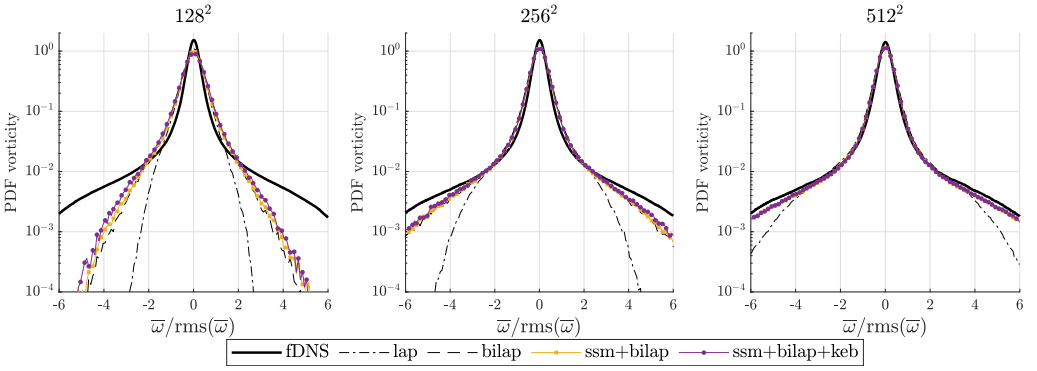

Figure 11: PDF of vorticity in a posteriori experiments compared to filtered DNS data. Time moment $t = 10$, $\overline{\Delta}/\Delta_g = \sqrt{6}$.

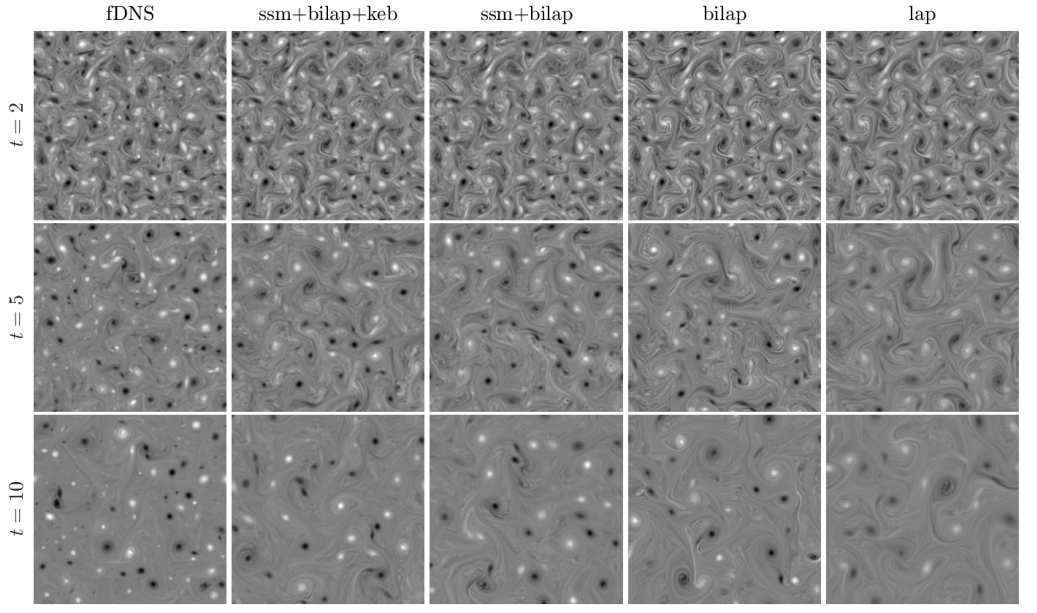

Figure 12: Snapshots of vorticity in a posteriori experiment at resolution 256^2 and $\overline{\Delta}/\Delta_g = \sqrt{6}$ compared to filtered DNS data. Colorbar range is $(-50, 50)$.

energy backscatter (`ssm+bilap+keb`). Although the last model correctly predicts the energy transfer spectrum at $t = 2$, an error in middle scales is gradually accumulated during the whole simulation at coarse resolution 128^2. At time $t = 10$, the whole backscattered energy is distributed over a few low wavenumbers; see figure 10, resolution 128^2, violet line. As will be shown in the next section, this problem can be more clearly studied in terms of enstrophy decay and Smagorinsky constant.

In figure 12, we show snapshots of vorticity for LES models at intermediate resolution (256^2) compared to fDNS data for one realization of initial condition. The models presented give robust numerical solutions: the vorticity field is smooth, and coherent structures and turbulent filaments are clearly identifiable.

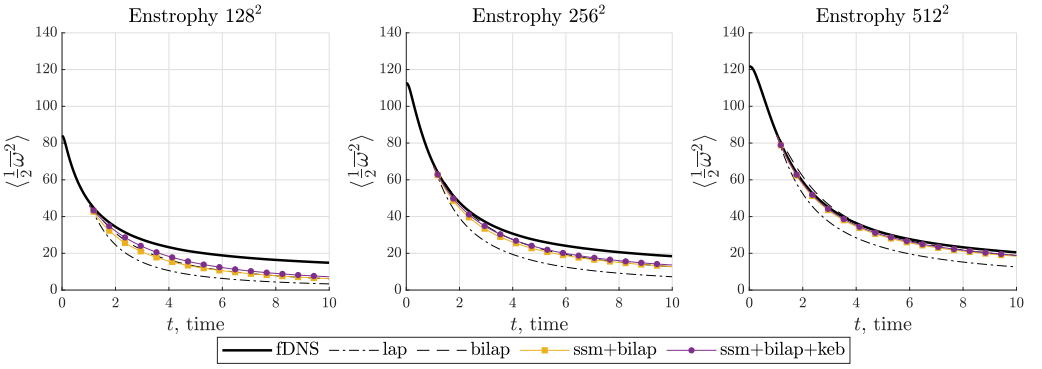

Figure 13: Enstrophy in a posteriori experiments compared to filtered DNS data, $\overline{\Delta}/\Delta_g = \sqrt{6}$.

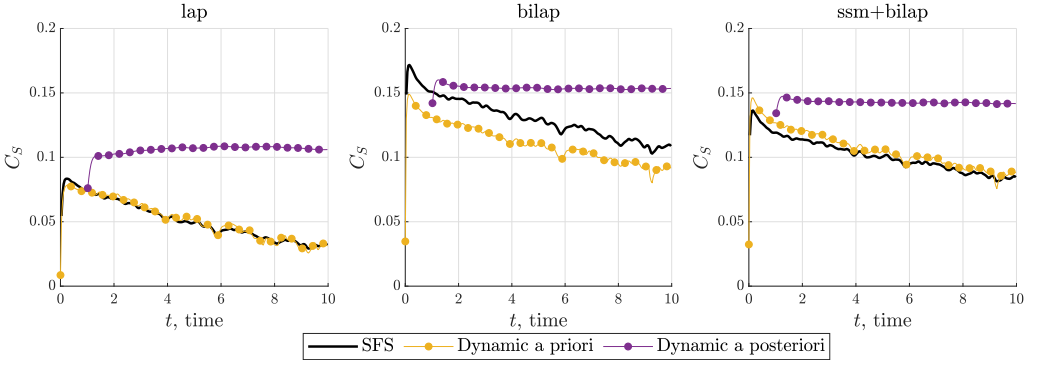

Figure 14: Black line – C_S estimated by enstrophy dissipation in a priori analysis, orange line – C_S estimated by dynamic model in a priori analysis. Violet line – C_S estimated by dynamic model in a posteriori experiment at resolution 128^2 and $\overline{\Delta}/\Delta_g = \sqrt{6}$.

4.3. *Smagorinsky constant*

The lack of energy in the middle scales at coarse resolution can be explained by the too rapid decay of enstrophy; see figure 13 (128^2). The model with the parameterization of kinetic energy backscatter `ssm+bilap+keb` only slightly improves this characteristic. A similar effect of KEB in 2D decaying turbulence has been reported in Thuburn *et al.* (2014). The enstrophy dissipation is controlled by the Smagorinsky constant. We have estimated the Smagorinsky constant in a priori analysis on the DNS grid based on the requirement that the SFS model should dissipate the correct amount of enstrophy:

$$C_S^2 = \frac{\langle \sigma_j \frac{\partial \overline{\omega}}{\partial x_j} \rangle}{\langle m_j^{lap}[\overline{\Delta}] \frac{\partial \overline{\omega}}{\partial x_j} \rangle}, \tag{4.1}$$

for `lap` model and similarly for the other SFS models. This constant is shown in figure 14 by a black line, and it decreases with time for the three SFS models presented. The decrease indicates the structure of turbulent flow changes, and there is no unique Smagorinsky constant suitable to any flow regime. In works (San 2014; Maulik & San 2017*d*,*a*), the Smagorinsky constant is estimated dynamically in a posteriori experiments for Laplacian viscosity. After an initial transition, it almost does not depend on time. We have found a similar behaviour: the Smagorinsky constant increases sharply immediately after the start of the experiment

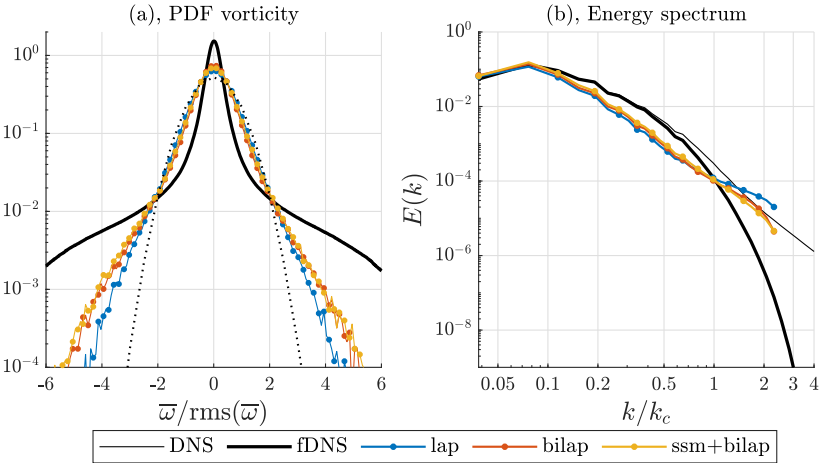

Figure 15: Experiments at resolution 128^2, $\overline{\Delta}/\Delta_g = \sqrt{6}$, $t = 10$. C_s is taken from a priori analysis. A dotted line has Gaussian PDF.

and then becomes significantly overestimated compared to a priori data and does not depend on time; see figure 14, violet line. The dynamically estimated Smagorinsky constant is also almost insensitive to the resolution (not shown).

The dynamic procedure includes an assumption that is generally not valid: the Smagorinsky constant is assumed to be scale invariant. As discussed above, decay of 2D turbulence is not self-similar, and this assumption is clearly false. There are various similar procedures to estimate the Smagorinsky constant without the need for scale invariance. In works (Meneveau & Lund 1997; Porté-Agel *et al.* 2000) scale-dependent dynamic model was proposed, where the Smagorinsky constant can depend on the filter width. In works (Maulik & San 2017*b*,*d*) "projection" of various approximations of SFS stress (ADM, SSM, and so on) onto viscosity kernel was proposed.

There could be a two reasons, why the dynamic procedure overestimates the Smagorinsky constant: either it is inaccurate when the base filter width does not correspond to a self-similar band of wavenumbers, or solution is distorted under the action of the SFS model, resulting in the wrong prediction. The Smagorinsky constant estimated dynamically in an a priori experiment on the DNS grid is shown in figure 14 by orange line. This line is much closer to a priori data computed based on the enstrophy dissipation. Thus, we come to the conclusion that the problem is not in the dynamic procedure, but in the transformation of the solution under the influence of the SFS model. Finally, we checked whether the a priori computed Smagorinsky constant can improve the simulation. We performed an experiment with the Smagorinsky constant defined by a priori data (black line in figure 14). The results are shown in figure 15. Middle scales are still underestimated, but the numerical noise arises, which is seen in the smallest scales in the energy spectrum and in the almost Gaussian vorticity PDF.

In the LES models studied, the crudest approximation was made for the cross stress. Based on the analysis performed in this section, we conclude that when the base filter width is of the order of the size of coherent vortices, the influence of the full SFS stress or its part (cross stress) on the solution cannot be simulated with the eddy viscosity model. In particular, an enstrophy cascade that is too strong develops, and this cascade is efficiently estimated by the dynamic model in an a posteriori experiment, leading to the excessive enstrophy dissipation. The change of the viscosity kernel from Smagorinsky to Leith (1996) model does not improve the energy spectrum in the middle scales (not shown). The Lagrangian dynamic

model (Meneveau *et al.* 1996) is able to estimate the Smagorinsky constant depending on the local structure of turbulent flow: low values of C_S for coherent vortices and large values for turbulent filaments. Experiments with this model do not show improvement in the energy spectrum in the middle scales (not shown).

5. Conclusions

Modern ocean general circulation models use subgrid parameterizations of unresolved quasi-2D turbulence, and these parameterizations are built on physical principles. In particular, dissipation of enstrophy is usually described by the bilaplacian eddy viscosity with the Smagorinsky coefficient, and the Smagorinsky constant is defined uniquely independent of the structure of resolved turbulent flow, $\nu = 0.06\Delta_g^4|S|$, where Δ_g – grid step; see Jansen *et al.* (2015, 2019); Griffies & Hallberg (2000). Parameterizations of kinetic energy backscatter (KEB) usually obey two main principles: they should have a spatial scale larger than the spatial scale of a dissipative operator, and they should return an amount of energy proportional to its dissipation (Jansen & Held 2014).

In this work, we studied enstrophy dissipation and kinetic energy backscatter parameterizations in a rigorous LES approach for the simplest example of 2D turbulent flow – decaying turbulence. The quality of LES models is assessed in terms of how they reproduce the statistical characteristics of the filtered DNS and of the SFS stress. To distinguish numerical errors from inaccuracy of the SFS model, we apply an explicit filtering approach and show that the LES models constructed possess grid-convergent turbulence statistics for fixed base filter width.

In a priori analysis of SFS stress with Gaussian filter, energy and enstrophy transfer spectra are shown to have a complex structure. In particular, there are bands of wavenumbers corresponding to dissipation and backscatter, and a substantial part of the enstrophy dissipation is concentrated in subfilter scales. We have supposed that accurate modelling of both transfer spectra is necessary to reproduce turbulence statistics of filtered DNS. SFS stress is decomposed into three parts (Leonard, cross, Reynolds) according to the Germano decomposition. The enstrophy transfer spectrum of the cross stress can be modelled with the bilaplacian eddy viscosity. Reynolds stress was shown to return energy on large scales, and its contribution to enstrophy transfer on small scales is negligible. Thus, its simplest approximation by a deconvolution procedure of the lowest order can be considered a parameterization of kinetic energy backscatter. This parameterization was shown to correlate highly with SFS stress (40-60%). Additionally, we have derived a lower bound estimate for the upscale transfer of energy from unresolved to resolved scales, which gives us "amplitude" of the backscatter.

Compared to usual KEB parameterizations, we have rigorously derived two main components of the parameterization: the model, which returns energy in the correct band of wavenumbers, and the procedure to estimate its amplitude. Both results rely on the well known approximations of SFS stress or its part. The role of Reynolds stress in contributing into upscale energy transfer in more complex flow regimes remains to be investigated in further studies. Our estimate of the amount of upscale energy transfer is applicable only for 2D decaying turbulence at high Reynolds numbers. However, we claim that finding similar estimates based on the approximation of the SFS stress for more complex flow regimes could give a significant improvement in the efficiency of KEB parameterizations. For example, Grooms *et al.* (2013) shows that energy exchange with SFS motions has a complex structure in quasi-geostrophic turbulence: an intergyre jet absorbs the energy of SFS motions, and SFS energy is created elsewhere in the basin.

We have proposed the three-component model consisting of the following parts: Leonard

stress, bilaplacian eddy viscosity with the Smagorinsky coefficient and KEB parameterization. The Smagorinsky constant is estimated using a standard dynamic procedure. The three-component model is compared to simpler dynamic models: Smagorinsky Laplacian, Smagorinsky bilaplacian and mixed model (Leonard stress and Smagorinsky bilaplacian).

Grid convergence analysis has shown that the minimum filter to grid width ratio required to obtain robust numerical solutions using dynamic procedure is $\overline{\Delta}/\Delta_g = \sqrt{6}$ (for second-order numerical schemes). This fact explains why applying dynamic models in 2D turbulence often leads to formation of numerical noise.

The three-component model in a posteriori experiments correctly describes enstrophy and energy transfer spectra of SFS stress, pointwise enstrophy flux and growth of resolved energy. With the refinement of the numerical grid (at fixed $\overline{\Delta}/\Delta_g = \sqrt{6}$) turbulence statistics of LES models presented converge to the filtered DNS data. The slowest convergence is found for the Smagorinsky Laplacian model. The most substantial impact of KEB parameterization on the resolved energy is found in the case when the base filter width is of the order of the size of coherent vortices. This spatial scale does not correspond to a self-similar region in the energy spectrum. In this case, all LES models presented underestimate the energy spectrum in the middle resolved scales. An accurate enstrophy dissipation model (mixed model) and KEB parameterization give almost no improvement in sustaining coherent vortices compared to the Smagorinsky bilaplacian eddy viscosity model. KEB parameterization leads to the accumulation of backscattered energy in a few low wavenumbers. Note that this case is the most interesting in ocean modelling, because mesoscale eddies often fall within a grid length scale, particularly at higher latitudes, see Hewitt *et al.* (2020).

Underestimation of the energy in the middle scales is connected to the too rapid decay of the enstrophy. In a priori analysis, we have shown that the Smagorinsky constant should decrease as coherent vortices develop, and dynamic models in an a priori experiment correctly predict this decrease. However, in a posteriori experiments, dynamic models overestimate the Smagorinsky constant, and the constant is almost insensitive to the structure of the turbulent flow and base filter width. An additional a posteriori experiment with the Smagorinsky constant given by a priori analysis led to the noisy solutions. Based on these findings, we have supposed that overestimation of the Smagorinsky constant is not related to the deficiency of the dynamic procedure, but it is related to the response of the LES model to the inaccurate SFS model.

Because the crudest approximation in the three-component model was made to the cross stress, we conclude that the cross stress cannot be replaced with the eddy viscosity model. Possibly, better results can be achieved for SFS models, which accurately reproduce cross stress (for example, the approximate deconvolution model). However, its spectral density is concentrated on subfilter scales, and it is very unlikely that such a model will be used in geophysical applications because of numerical stability reasons.

Summarizing the results of this work and previous studies (San 2014; Maulik & San 2017*d*), the Smagorinsky constant predicted by the dynamic procedure in a posteriori experiments is almost insensitive to the grid resolution, Reynolds number and structure of the resolved flow. To achieve similar results, one can use a unique Smagorinsky constant for any flow regime. In our experiments, the Smagorinsky constant in bilaplacian model is $C_S \approx 0.155$ for base filter width $\overline{\Delta}/\Delta_g = \sqrt{6}$, which gives eddy viscosity coefficient $\nu = (C_s\sqrt{6}\Delta_g)^4|S| \approx 0.02\Delta_g^4|S|$. Although we use quite a wide base filter, this coefficient is still lower than the coefficient routinely used in ocean models ($\nu = 0.06\Delta_g^4|S|$). In ocean models, except for accurate modelling of the enstrophy cascade, there are numerous constraints limiting the minimum value of the eddy viscosity coefficient, such as preserving

the grid-Reynolds number and resolving a viscous boundary layer; see Griffies & Hallberg (2000).

We have shown that the role of KEB parameterization in sustaining coherent vortices in 2D decaying turbulence is insignificant, and backscattered energy accumulates in a few low wavenumbers. In ocean mesoscale turbulence, the role of KEB parameterization increases because the energy level defines the strength of the eddy heat and salinity fluxes, and they, in turn, define the release of available potential energy from the mean flow. However, based on the results of this work, we suggest that KEB parameterization will not necessary improve the dynamics of coherent structures. For example, in Perezhogin (2020), we shown that KEB parameterization energizes eddying motions, but they do not organize into a western boundary current extension. Note that the correct reproduction of coherent structures is expected to be a key property, required to correctly describe resolved eddy mixing (Kong & Jansen 2017).

Funding. The study was performed at Institute of Numerical Mathematics. Development of subgrid closures was supported by the Moscow Center for Fundamental and Applied Mathematics (agreement no. 075-15-2019-1624 with the Ministry of Education and Science of the Russian Federation). An analysis of energy transfer was supported by the Russian Science Foundation (project 21-71-30023).

Declaration of interests. The authors report no conflict of interest.

Author ORCID. P.A. Perezhogin, https://orcid.org/0000-0003-2098-3457

REFERENCES

Arakawa, Akio 1997 Computational design for long-term numerical integration of the equations of fluid motion: Two-dimensional incompressible flow. part i. *Journal of computational physics* **135** (2), 103–114.

Arakawa, Akio & Lamb, Vivian R 1977 Computational design of the basic dynamical processes of the ucla general circulation model. *General circulation models of the atmosphere* **17** (Supplement C), 173–265.

Bachman, Scott D, Fox-Kemper, Baylor & Pearson, Brodie 2017 A scale-aware subgrid model for quasi-geostrophic turbulence. *Journal of Geophysical Research: Oceans* **122** (2), 1529–1554.

Bardina, Jorge, Ferziger, J & Reynolds, W 1980 Improved subgrid-scale models for large-eddy simulation. In *13th fluid and plasmadynamics conference*, p. 1357.

Bardino, J, Ferziger, Joel H & Reynolds, William C 1983 Improved turbulence models based on large eddy simulation of homogeneous, incompressible turbulent flows. *Stanford Univ. Report* .

Bartello, Peter & Warn, Tom 1996 Self-similarity of decaying two-dimensional turbulence. *Journal of Fluid Mechanics* **326**, 357–372.

Batchelor, George K 1969 Computation of the energy spectrum in homogeneous two-dimensional turbulence. *The Physics of Fluids* **12** (12), II–233.

Beck, Andrea, Flad, David & Munz, Claus-Dieter 2019 Deep neural networks for data-driven les closure models. *Journal of Computational Physics* **398**, 108910.

Berloff, Pavel 2018 Dynamically consistent parameterization of mesoscale eddies. part iii: Deterministic approach. *Ocean Modelling* **127**, 1–15.

Berner, Judith, Shutts, GJ, Leutbecher, M & Palmer, TN 2009 A spectral stochastic kinetic energy backscatter scheme and its impact on flow-dependent predictability in the ecmwf ensemble prediction system. *Journal of the Atmospheric Sciences* **66** (3), 603–626.

Bose, Sanjeeb T, Moin, Parviz & You, Donghyun 2010 Grid-independent large-eddy simulation using explicit filtering. *Physics of Fluids* **22** (10), 105103.

Bouchet, Freddy 2003 Parameterization of two-dimensional turbulence using an anisotropic maximum entropy production principle. *arXiv preprint cond-mat/0305205* .

Buxton, ORH, Laizet, S & Ganapathisubramani, B 2011 The interaction between strain-rate and rotation in shear flow turbulence from inertial range to dissipative length scales. *Physics of Fluids* **23** (6), 061704.

Carati, Daniele, Winckelmans, Grégoire S & Jeanmart, Hervé 2001 On the modelling of the subgrid-

scale and filtered-scale stress tensors in large-eddy simulation. *Journal of Fluid Mechanics* **441**, 119.

Cerutti, Stefano, Meneveau, Charles & Knio, Omar M 2000 Spectral and hyper eddy viscosity in high-reynolds-number turbulence. *Journal of Fluid Mechanics* **421**, 307–338.

Chasnov, JR 1997 On the decay of two-dimensional homogeneous turbulence. *Physics of Fluids* **9** (1), 171–180.

Chen, Shiyi, Ecke, Robert E, Eyink, Gregory L, Rivera, Michael, Wan, Minping & Xiao, Zuoli 2006 Physical mechanism of the two-dimensional inverse energy cascade. *Physical review letters* **96** (8), 084502.

Chen, Shiyi, Ecke, Robert E, Eyink, Gregory L, Wang, Xin & Xiao, Zuoli 2003 Physical mechanism of the two-dimensional enstrophy cascade. *Physical review letters* **91** (21), 214501.

Chow, Fotini Katopodes & Moin, Parviz 2003 A further study of numerical errors in large-eddy simulations. *Journal of Computational Physics* **184** (2), 366–380.

Clark, Robert A, Ferziger, J & Reynolds, W 1979 Evaluation of subgrid-scale models using an. *J. Fluid Mech* **91** (part 1), 1–16.

Dubinkina, Svetlana & Frank, Jason 2007 Statistical mechanics of arakawa's discretizations. *Journal of Computational Physics* **227** (2), 1286–1305.

Dymnikov, VP & Perezhogin, PA 2018 Systems of hydrodynamic type that approximate two-dimensional ideal fluid equations. *Izvestiya, Atmospheric and Oceanic Physics* **54** (3), 232–241.

Fox-Kemper, B & Menemenlis, D 2008 Can large eddy simulation techniques improve mesoscale rich ocean models. *Ocean modeling in an eddying regime* **177**, 319–337.

Frederiksen, Jorgen S & Davies, Antony G 1997 Eddy viscosity and stochastic backscatter parameterizations on the sphere for atmospheric circulation models. *Journal of the atmospheric sciences* **54** (20), 2475–2492.

Frederiksen, Jorgen S, Dix, Martin R & Davies, Antony G 2003 The effects of closure-based eddy diffusion on the climate and spectra of a gcm. *Tellus A: Dynamic Meteorology and Oceanography* **55** (1), 31–44.

Frederiksen, Jorgen S & Kepert, Steven M 2006 Dynamical subgrid-scale parameterizations from direct numerical simulations. *Journal of the atmospheric sciences* **63** (11), 3006–3019.

Frederiksen, Jorgen S, Kitsios, Vassili, O'Kane, Terence J & Zidikheri, Meelis J 2017 Stochastic subgrid modelling for geophysical and three-dimensional turbulence. In *Nonlinear and stochastic climate dynamics*, pp. 241–275. Cambridge University Press.

Frederiksen, Jorgen S, O'Kane, Terence J & Zidikheri, Meelis J 2012 Stochastic subgrid parameterizations for atmospheric and oceanic flows. *Physica Scripta* **85** (6), 068202.

Frigo, Matteo & Johnson, Steven G 1998 Fftw: An adaptive software architecture for the fft. In *Proceedings of the 1998 IEEE International Conference on Acoustics, Speech and Signal Processing, ICASSP'98 (Cat. No. 98CH36181)*, , vol. 3, pp. 1381–1384. IEEE.

Germano, Massimo 1986 A proposal for a redefinition of the turbulent stresses in the filtered navier–stokes equations. *The Physics of fluids* **29** (7), 2323–2324.

Germano, Massimo 1992 Turbulence: the filtering approach. *Journal of Fluid Mechanics* **238**, 325–336.

Germano, Massimo, Piomelli, Ugo, Moin, Parviz & Cabot, William H 1991 A dynamic subgrid-scale eddy viscosity model. *Physics of Fluids A: Fluid Dynamics* **3** (7), 1760–1765.

Ghosal, Sandip 1996 An analysis of numerical errors in large-eddy simulations of turbulence. *Journal of Computational Physics* **125** (1), 187–206.

Ghosal, Sandip, Lund, Thomas S, Moin, Parviz & Akselvoll, K 1995 A dynamic localization model for large-eddy simulation of turbulent flows. *J. Fluid Mech* **286**, 229–255.

Graham, Jonathan Pietarila & Ringler, Todd 2013 A framework for the evaluation of turbulence closures used in mesoscale ocean large-eddy simulations. *Ocean Modelling* **65**, 25–39.

Griffies, Stephen M & Hallberg, Robert W 2000 Biharmonic friction with a smagorinsky-like viscosity for use in large-scale eddy-permitting ocean models. *Monthly Weather Review* **128** (8), 2935–2946.

Grooms, Ian, Lee, Yoonsang & Majda, Andrew J 2015 Numerical schemes for stochastic backscatter in the inverse cascade of quasigeostrophic turbulence. *Multiscale Modeling & Simulation* **13** (3), 1001–1021.

Grooms, Ian, Nadeau, Louis-Philippe & Smith, K Shafer 2013 Mesoscale eddy energy locality in an idealized ocean model. *Journal of physical oceanography* **43** (9), 1911–1923.

Guan, Yifei, Chattopadhyay, Ashesh, Subel, Adam & Hassanzadeh, Pedram 2021 Stable a posteriori

les of 2d turbulence using convolutional neural networks: Backscattering analysis and generalization to higher re via transfer learning. *arXiv preprint arXiv:2102.11400* .

Gullbrand, Jessica & Chow, Fotini Katopodes 2003 The effect of numerical errors and turbulence models in large-eddy simulations of channel flow, with and without explicit filtering. *Journal of Fluid Mechanics* **495**, 323.

Hewitt, Helene T, Roberts, Malcolm, Mathiot, Pierre, Biastoch, Arne, Blockley, Ed, Chassignet, Eric P, Fox-Kemper, Baylor, Hyder, Pat, Marshall, David P, Popova, Ekaterina & others 2020 Resolving and parameterising the ocean mesoscale in earth system models. *Current Climate Change Reports* pp. 1–16.

Horiuti, Kiyosi 1997 A new dynamic two-parameter mixed model for large-eddy simulation. *Physics of Fluids* **9** (11), 3443–3464.

Hughes, Thomas JR, Wells, Garth N & Wray, Alan A 2004 Energy transfers and spectral eddy viscosity in large-eddy simulations of homogeneous isotropic turbulence: Comparison of dynamic smagorinsky and multiscale models over a range of discretizations. *Physics of Fluids* **16** (11), 4044–4052.

Jansen, Malte F, Adcroft, Alistair, Khani, Sina & Kong, Hailu 2019 Toward an energetically consistent, resolution aware parameterization of ocean mesoscale eddies. *Journal of Advances in Modeling Earth Systems* **11** (8), 2844–2860.

Jansen, Malte F & Held, Isaac M 2014 Parameterizing subgrid-scale eddy effects using energetically consistent backscatter. *Ocean Modelling* **80**, 36–48.

Jansen, Malte F, Held, Isaac M, Adcroft, Alistair & Hallberg, Robert 2015 Energy budget-based backscatter in an eddy permitting primitive equation model. *Ocean Modelling* **94**, 15–26.

Juricke, S, Danilov, S, Koldunov, N, Oliver, M, Sein, DV, Sidorenko, D & Wang, Q 2020*a* A kinematic kinetic energy backscatter parametrization: From implementation to global ocean simulations. *Journal of Advances in Modeling Earth Systems* **12** (12), e2020MS002175.

Juricke, Stephan, Danilov, Sergey, Koldunov, Nikolay, Oliver, Marcel & Sidorenko, Dmitry 2020*b* Ocean kinetic energy backscatter parametrization on unstructured grids: Impact on global eddy-permitting simulations. *Journal of Advances in Modeling Earth Systems* **12** (1), e2019MS001855.

Juricke, Stephan, Danilov, Sergey, Kutsenko, Anton & Oliver, Marcel 2019 Ocean kinetic energy backscatter parametrizations on unstructured grids: Impact on mesoscale turbulence in a channel. *Ocean Modelling* **138**, 51–67.

Kitsios, V, Frederiksen, Jorgen S & Zidikheri, MJ 2013 Scaling laws for parameterisations of subgrid eddy–eddy interactions in simulations of oceanic circulations. *Ocean Modelling* **68**, 88–105.

Kong, Hailu & Jansen, Malte F 2017 The eddy diffusivity in barotropic β-plane turbulence. *Fluids* **2** (4), 54.

Kraichnan, Robert H 1967 Inertial ranges in two-dimensional turbulence. *The Physics of Fluids* **10** (7), 1417–1423.

Kraichnan, Robert H 1976 Eddy viscosity in two and three dimensions. *Journal of the atmospheric sciences* **33** (8), 1521–1536.

Kurz, Marius & Beck, Andrea 2020 A machine learning framework for les closure terms. *arXiv preprint arXiv:2010.03030* .

Langford, Jacob A & Moser, Robert D 1999 Optimal les formulations for isotropic turbulence. *Journal of fluid mechanics* **398**, 321–346.

Layton, William J & Rebholz, Leo G 2012 *Approximate deconvolution models of turbulence: analysis, phenomenology and numerical analysis*, , vol. 2042. Springer Science & Business Media.

Leith, CE 1996 Stochastic models of chaotic systems. *Physica D: Nonlinear Phenomena* **98** (2-4), 481–491.

Leith, Cecil E 1968 Diffusion approximation for two-dimensional turbulence. *The Physics of Fluids* **11** (3), 671–672.

Leonard, A 1997 Large-eddy simulation of chaotic convection and beyond. In *35th Aerospace Sciences Meeting and Exhibit*, p. 204.

Leslie, DC & Quarini, GL 1979 The application of turbulence theory to the formulation of subgrid modelling procedures. *Journal of fluid mechanics* **91** (1), 65–91.

Lilly, Douglas K 1967 The representation of small-scale turbulence in numerical simulation experiments. *IBM Form* pp. 195–210.

Lund, TS 1997 On the use of discrete filters for large eddy simulation. *Annual Research Briefs* pp. 83–95.

Lund, TS 2003 The use of explicit filters in large eddy simulation. *Computers & Mathematics with Applications* **46** (4), 603–616.

Maulik, Romit & San, Omer 2016 Dynamic modeling of the horizontal eddy viscosity coefficient for quasigeostrophic ocean circulation problems. *Journal of Ocean Engineering and Science* **1** (4), 300–324.

Maulik, R & San, O 2017*a* A dynamic framework for functional parameterisations of the eddy viscosity coefficient in two-dimensional turbulence. *International Journal of Computational Fluid Dynamics* **31** (2), 69–92.

Maulik, Romit & San, Omer 2017*b* A novel dynamic framework for subgrid scale parametrization of mesoscale eddies in quasigeostrophic turbulent flows. *Computers & Mathematics with Applications* **74** (3), 420–445.

Maulik, Romit & San, Omer 2017*c* Resolution and energy dissipation characteristics of implicit les and explicit filtering models for compressible turbulence. *Fluids* **2** (2), 14.

Maulik, Romit & San, Omer 2017*d* A stable and scale-aware dynamic modeling framework for subgrid-scale parameterizations of two-dimensional turbulence. *Computers & Fluids* **158**, 11–38.

Maulik, Romit, San, Omer, Rasheed, Adil & Vedula, Prakash 2019 Subgrid modelling for two-dimensional turbulence using neural networks. *Journal of Fluid Mechanics* **858**, 122–144.

McWilliams, James C 1984 The emergence of isolated, coherent vortices in turbulent flow. In *AIP Conference Proceedings*, , vol. 106, pp. 205–221. American Institute of Physics.

Meneveau, Charles & Katz, Joseph 2000 Scale-invariance and turbulence models for large-eddy simulation. *Annual Review of Fluid Mechanics* **32** (1), 1–32.

Meneveau, Charles & Lund, Thomas S 1997 The dynamic smagorinsky model and scale-dependent coefficients in the viscous range of turbulence. *Physics of fluids* **9** (12), 3932–3934.

Meneveau, Charles, Lund, Thomas S & Cabot, William H 1996 A lagrangian dynamic subgrid-scale model of turbulence. *Journal of fluid mechanics* **319**, 353–385.

Moin, Parviz & Kim, John 1982 Numerical investigation of turbulent channel flow. *Journal of fluid mechanics* **118**, 341–377.

Mortikov, Evgeny V, Glazunov, Andrey V & Lykosov, Vasily N 2019 Numerical study of plane couette flow: turbulence statistics and the structure of pressure–strain correlations. *Russian Journal of Numerical Analysis and Mathematical Modelling* **34** (2), 119–132.

Nadiga, BT 2008 Orientation of eddy fluxes in geostrophic turbulence. *Philosophical Transactions of the Royal Society A: Mathematical, Physical and Engineering Sciences* **366** (1875), 2489–2508.

Pawar, Suraj, San, Omer, Rasheed, Adil & Vedula, Prakash 2020 A priori analysis on deep learning of subgrid-scale parameterizations for kraichnan turbulence. *Theoretical and Computational Fluid Dynamics* **34** (4), 429–455.

Pearson, Brodie, Fox-Kemper, Baylor, Bachman, Scott & Bryan, Frank 2017 Evaluation of scale-aware subgrid mesoscale eddy models in a global eddy-rich model. *Ocean Modelling* **115**, 42–58.

Perezhogin, Pavel A 2020 Testing of kinetic energy backscatter parameterizations in the nemo ocean model. *Russian Journal of Numerical Analysis and Mathematical Modelling* **35** (2), 69–82.

Perezhogin, Pavel A, Glazunov, Andrey V & Gritsun, Andrey S 2019 Stochastic and deterministic kinetic energy backscatter parameterizations for simulation of the two-dimensional turbulence. *Russian Journal of Numerical Analysis and Mathematical Modelling* **34** (4), 197–213.

Perezhogin, Pavel A, Glazunov, Andrey V, Mortikov, Evgeny V & Dymnikov, Valentin P 2017 Comparison of numerical advection schemes in two-dimensional turbulence simulation. *Russian Journal of Numerical Analysis and Mathematical Modelling* **32** (1), 47–60.

Pomraning, Eric & Rutland, Christopher J 2002 Dynamic one-equation nonviscosity large-eddy simulation model. *AIAA journal* **40** (4), 689–701.

Porté-Agel, Fernando, Meneveau, Charles & Parlange, Marc B 2000 A scale-dependent dynamic model for large-eddy simulation: application to a neutral atmospheric boundary layer. *Journal of Fluid Mechanics* **415** (ARTICLE), 261–284.

Rivera, MK, Daniel, WB, Chen, SY & Ecke, RE 2003 Energy and enstrophy transfer in decaying two-dimensional turbulence. *Physical review letters* **90** (10), 104502.

Sagaut, Pierre 2006 *Large eddy simulation for incompressible flows: an introduction*. Springer Science & Business Media.

Sagaut, Pierre & Grohens, R 1999 Discrete filters for large eddy simulation. *International Journal for Numerical Methods in Fluids* **31** (8), 1195–1220.

San, Omer 2014 A dynamic eddy-viscosity closure model for large eddy simulations of two-dimensional decaying turbulence. *International Journal of Computational Fluid Dynamics* **28** (6-10), 363–382.

Sarwar, Mahfuz, Cleary, MJ, Moinuddin, KAM & Thorpe, GR 2017 On linking the filter width to

the boundary layer thickness in explicitly filtered large eddy simulations of wall bounded flows. *International Journal of Heat and Fluid Flow* **65**, 73–89.

Schilling, Oleg & Zhou, Ye 2002 Analysis of spectral eddy viscosity and backscatter in incompressible, isotropic turbulence using statistical closure theory. *Physics of Fluids* **14** (3), 1244–1258.

Schumann, Ulrich 1995 Stochastic backscatter of turbulence energy and scalar variance by random subgrid-scale fluxes. *Proceedings of the Royal Society of London. Series A: Mathematical and Physical Sciences* **451** (1941), 293–318.

Skamarock, William C, Klemp, Joseph B, Dudhia, Jimy, Gill, David O, Barker, Dale M, Wang, Wei & Powers, Jordan G 2008 A description of the advanced research wrf version 3. ncar technical note-475+ str .

Smagorinsky, Joseph 1963 General circulation experiments with the primitive equations: I. the basic experiment. *Monthly weather review* **91** (3), 99–164.

Stoffer, Robin, van Leeuwen, Caspar M, Podareanu, Damian, Codreanu, Valeriu, Veerman, Menno A, Janssens, Martin, Hartogensis, Oscar K & van Heerwaarden, Chiel C 2020 Development of a large-eddy simulation subgrid model based on artificial neural networks: a case study of turbulent channel flow. *Geoscientific Model Development Discussions* pp. 1–29.

Stolz, S, Adams, Nikolaus A & Kleiser, Leonhard 2001 An approximate deconvolution model for large-eddy simulation with application to incompressible wall-bounded flows. *Physics of fluids* **13** (4), 997–1015.

Thuburn, John, Kent, James & Wood, Nigel 2014 Cascades, backscatter and conservation in numerical models of two-dimensional turbulence. *Quarterly Journal of the Royal Meteorological Society* **140** (679), 626–638.

Verstappen, Roel 2011 When does eddy viscosity damp subfilter scales sufficiently? *Journal of Scientific Computing* **49** (1), 94–110.

Vreman, AW 2004 An eddy-viscosity subgrid-scale model for turbulent shear flow: Algebraic theory and applications. *Physics of fluids* **16** (10), 3670–3681.

Vreman, Bert, Geurts, Bernard & Kuerten, Hans 1997 Large-eddy simulation of the turbulent mixing layer. *Journal of fluid mechanics* **339**, 357–390.

Winckelmans, Grégoire S, Wray, Alan A, Vasilyev, Oleg V & Jeanmart, Hervé 2001 Explicit-filtering large-eddy simulation using the tensor-diffusivity model supplemented by a dynamic smagorinsky term. *Physics of Fluids* **13** (5), 1385–1403.

Xie, Chenyue, Wang, Jianchun & Weinan, E 2020 Modeling subgrid-scale forces by spatial artificial neural networks in large eddy simulation of turbulence. *Physical Review Fluids* **5** (5), 054606.

Zidikheri, Meelis J & Frederiksen, Jorgen S 2009 Stochastic subgrid parameterizations for simulations of atmospheric baroclinic flows. *Journal of the Atmospheric Sciences* **66** (9), 2844–2858.